Response and component characterization of semi-rigid connections to tubular columns under axial loads

Y. Liu, C. Málaga-Chuquitaype, A. Y. Elghazouli

Department of Civil and Environmental Engineering, Imperial College London, UK

Abstract

This paper examines the behaviour of open beam-to-tubular column bolted connections with angles subjected to direct tension and compression. Experimental and numerical studies as well as simplified mechanical assessments are presented. The response of seven tension tests and six compression tests on blind-bolted angle connections and combined channel/angle configurations are described and discussed in detail. Firstly, the experimental set-up, connection details and material properties are introduced followed by a detailed account of the results and observations from the tests. Based on the experimental results, the main behavioural patterns are identified and the salient response characteristics such as stiffness, capacity and failure mechanism are examined. It is shown that, for Hollo-bolted details, the distance between the blind-bolt and beam flange, the angle thickness and the column thickness have significant effects on the initial stiffness and tensile capacity of the connection. In addition, in the case of reverse channel connections, a direct relationship is deduced between the thickness of the channel component and the connection stiffness and capacity. It is also shown that the inelastic axial mechanisms exhibited by these types of connections are largely determined by the relative widths of the column/reverse channel and beam/angle components. Complementary finite element simulations are presented and utilised, together with the experimental findings, to highlight the main inelastic response characteristics for these forms of connections under direct axial action. Finally, the component-based method is extended to deal with angle connections between open beams and tubular columns employing Hollo-bolts or reverse channel components. To this end, expressions for the estimation of connection stiffness and capacity under axial actions are proposed and validated.

Keywords: blind-bolted angle connections, combined channel/angle connections, tension action, compression behaviour, component models.

1. Introduction

Hollow structural sections (HSS) offer an effective choice as column members due to both their structural efficiency and architectural appeal. Nevertheless, the difficulties associated with the lack of access for the installation of conventional bolts have often resulted in the under exploitation of the HSS merits. This situation is aggravated by the relative lack of research and

design guidance for bolted angle connections with tubes. In contrast, the behaviour of open beam-to-open column joints with rigid or semi-rigid details has been extensively studied [1-3] and current European standards [4] incorporate rules for determining their stiffness and resistance.

The costs associated with the construction, inspection and maintenance of fully welded details have motivated the development of other connection alternatives such as the flowdrill process [5-7] and special bolts with sleeves designed to expand inside the tube [8-10]. A simpler blind-bolt design is that proposed by Lindapter International [11] through the development of the Hollo-bolt. In particular, the avoidance of close tolerance holes and specialized installation equipment renders the use of Hollo-bolts attractive. To this end, a number of experimental studies have been carried out on Hollo-bolted T-stubs and connections subjected mainly to bending [7, 12-14]. France et al. [7] carried out monotonic tests on three *end-plate* joints with blind-bolts and flowdrill bolts and reported adequate connection performance. Nevertheless, issues of practicality make the application of flowdrilling cumbersome hindering its wider use. Barnet et al. [12-13] performed a review of different blind-bolting alternatives and carried out an experimental study on blind-bolted T-stubs and connections using Hollo-bolts. To improve the clamping mechanism, a modified blind-bolt, referred to as the Reverse Mechanism Hollo-Bolt (RMHB) was proposed. More recently, Elghazouli et al. [14] performed an experimental investigation into the monotonic and cyclic behaviour of *top and seat* as well as *top, seat and web angle* connections Hollo-bolted to structural hollow columns. It was shown that the grade of the Hollo-bolt, coupled with the gauge distance between the Hollo-bolt and beam flange, have a most notable effect on the flexural response of this type of connection. Nevertheless, a comprehensive characterization of the full axial force-displacement relationship of Hollo-bolted connections to tubes has not been performed, particularly under compressive loads.

Another alternative for bolted connections between open beams and tubular columns is that offered by combined channel/angle configurations, in which a channel section is shop-welded at the legs end to the face of the column. The channel face is then connected on-site to the open beam by means of any conventional bolted detail. Despite its versatility, there is a lack of experimental studies on reverse channel configurations. Ding and Wang [15] compared the fire resistance of four end-plate reverse channel connections with other open beam-to-filled tubular column connection details. This study concluded that reverse channel connections can offer the best structural behaviour and cost-effectiveness among the different details considered. Málaga-Chuquitaype and Elghazouli [16] carried out an experimental study into the flexural behaviour of combined channel/angle connections including *top and seat* as well as *top, seat and web angle* details under monotonic and cyclic loading. It was observed that the flexibility of the reverse channel component has a direct influence on both the initial rotational stiffness and moment capacity of the connection, and the three main inelastic mechanism exhibited by this type of connection were identified. Nevertheless, as with blind-bolted details, there is a dearth of

experimental studies on the performance of combined channel/angle joints under other forms of severe loading conditions such as direct tension or compression.

Many studies have been carried out on the numerical simulation of semi-rigid connections incorporating conventional bolts [17-21]. Krishnamurthy [17] first used the finite element (FE) method to estimate the moment-rotation response of steel bolted *end-plate* connections. Citipitioglu et al. [18] presented a new displacement-based 3D FE model constructed in ABAQUS [22] able to predict the behaviour of partially-restrained connections; the effects of slip were incorporated by defining contact surfaces, and bolt pretension was applied by means of equivalent bolt shortening deformation. In contrast, Kishi et al. [19] directly applied the bolt pretension via a special scheme developed within ABAQUS. Similarly, several researchers have used FE analysis to study the behaviour of bolted angle connections subject to combined shear and moment as well as combined axial and bending actions [20-21]. Recently, Wang et al. [23] developed theoretical and numerical models within ANSYS [24] to investigate the tension behaviour of the Hollo-bolted T-stubs. However, similar detailed models for the simulation of blind-bolted or reverse channel joints with angles are still lacking.

A number of studies have also been carried out on the experimental response and analytical modelling of semi-rigid connections incorporating conventional bolts [19, 25-27]. However, these findings cannot be directly applied to Hollo-bolted details with angles due to the significant influence of contact phenomena and complex component interactions arising from the inherent rotational flexibility of the Hollo-bolt [14, 28]. Importantly, it has also been shown that when relatively stiff angles are provided, significant plastic deformations accumulate in the Hollo-bolt which can eventually lead to failure of the connection by bolt pull-out at large rotational demands [14]. Despite these significant differences between standard and Hollo-bolted details, analytical research on the response prediction of blind-bolted connections to tubular columns is still limited, in particular for joints with angles. Ghobarah et al. [29] suggested a model for the estimation of the initial stiffness and capacity of blind-bolted end-plate connections between open beams and tubular columns employing High Strength Blind-bolts [5, 8]. Wang et al. [23] investigated the behaviour of Hollo-bolted T-stubs and proposed an analytical model for the evaluation of their initial stiffness. More recently, Málaga-Chuquitaype and Elghazouli proposed and validated a component-based mechanical model for blind-bolted [28] and reverse channel [30] angle connections able to trace their full monotonic and cyclic moment-rotation response. Although general in form, none of these models have been validated against significant tensile or compressive joint deformations.

It can be noted from the above discussion that although the flexural response of semi-rigid connections to tubes has been reasonably well established, there is a need for a detailed characterization of their axial behaviour. Furthermore, it has been shown that under column removal design scenarios [31], significant levels of axial action are imposed onto the connections and that this has a strong influence on the structure survivability of the structure. Accordingly, there is a clear need for characterising the response of connections between open beams and

tubular columns subjected to direct axial forces. This paper deals with the behaviour of two cost-effective and practical connections subjected to direct tension and compression by means of experimental and numerical studies as well as simplified mechanical analyses. It describes and discusses the results of seven tension tests and six compression tests on Hollo-bolted angle connections and combined channel/angle details. The experimental set-up, connection configurations and material properties are first introduced followed by an overview of the results and observations from the tests. Based on the experimental results, the main behavioural patterns are discussed and the key response characteristics such as stiffness, capacity and failure mechanism are examined. Finite element models are developed and validated. It is demonstrated that these models can provide a realistic representation of the response of semi-rigid angle connections subjected to axial actions. Finally, this paper extends the component-based method to open beam-to tubular column angle connections employing Hollo-bolts or reverse channel components. The relevant component-based expressions for the determination of tension and compression stiffness and capacities are thus proposed. It is important to note that although the focus of this paper is on axial response, the component characterizations developed are also directly relevant to moment as well as combined moment/axial loading conditions.

2. Experimental programme

2.1 Testing set-up and specimen details

Figure 1 shows the experimental set-up used for testing bolted angle connections under tension. Previous numerical investigations [32] have shown that for the connection details studied herein the column length does not have an influence on the connection response under tensile action. Therefore, a 1500 mm length column was employed in all tensile specimens to suit laboratory constraints. The column was fixed at both ends by means of four 125 mm thickness clamping plates, as depicted in Figure 1. A hydraulic actuator operating in displacement control was connected to the beam top end in order to apply vertical deformations. The displacement at the top of the beam was gradually increased, at a rate of ≈ 0.5 mm/min, up to failure of the specimen or until the actuator capacity was reached at around 700 kN.

The test set-up used for the bolted angle connections under compression is depicted in Figure 2. The tubular column was fixed at both ends by two 50 mm clamping plates. To prevent buckling effects within the beam, a short beam of 125 mm length was employed. Displacements were applied to the specimen via a vertical actuator connected to the top surface of the beam. A maximum displacement of 25 mm, representative of large levels of local deformation, was applied to all compression specimens.

The applied vertical displacement and corresponding vertical force were recorded by the load cell and transducer incorporated within the actuator. Strain gauges were used to monitor the strains at expected inelastic regions within the angles and columns. The verticality of the load

was monitored through displacement transducers, while other transducers were employed to measure displacements at selected points within the column and angle components.

Seven tension tests were performed: four blind-bolted connection specimens and three reverse channel details. Similarly, six specimens were tested under compression action: three blind-bolted angle details and three combined channel/angle specimens. Table 1 summarizes the test series, including the geometric details of the connection as well as the column and beam sizes. T is used to refer to *Tension specimens* (T1 to T7) and C to *Compression specimens* (C1 to C6). Figure 3 depicts the connection configurations studied (Type A, Type B and Type C). In table 1, UB and SHS stand for Universal Beam and Square Hollow Section, respectively; while L refers to angle component. Importantly, the reverse channel components used in combined channel/angle configurations were obtained from SHS by longitudinal cutting. Table 1 gives the dimension of the SHS from which the reverse channels were obtained.

Grade 10.9 M16 standard bolts were employed to connect the beam flange and angle as well as the reverse channel and angle components, while Grade 10.9 M16 Hollo-bolts were utilized between the tubular column and angles. Tightening torques of 315 and 244 Nm were applied to the standard and Hollo-bolts, respectively, by means of calibrated external torque devices; these torque levels are assumed to produce preloads of 110 and 85 kN for standard and Hollo-bolts, respectively, based on manufacturer information. The angles were made of Grade S275 steel whilst S375 was adopted for beams and columns. The mean yield stress values and ultimate strength for the angle, beam and column components as obtained from at least three coupon tests are presented in Table 2. The axial capacity of Grade 10.9 M16 Hollo-bolts can be assumed as 78 kN based on the experimental tension-deformation relationships presented by Elghazouli et al. [14]. Also, hardness test were employed to determine the material characteristics of the Hollo-bolt sleeves and the results are presented in Table 2. Fillet welding with a throat thickness of 10 mm was used to connect the column and the reverse channel throughout the length of the channel external face.

2.2 Results and observations from tension tests

Table 3 summarizes the main response parameters obtained from the tensile tests on blind-bolted and reverse channel connections, while Figures 4-9 present the deformation patterns and tension force-displacement relationships. The initial stiffness and yield force presented in Table 3 were obtained from a bilinear idealization of the experimental force-displacement relationship by maintaining the same initial elastic stiffness and assuming conservation of work. These definitions are consistently applied throughout the paper. In subsequent sections, the experimental results and observations from the four blind-bolted angle connection specimens and the three combined channel/angle connection specimens are presented and discussed by considering the influence of the following parameters on the connection behaviour under tensile force: (i) gauge distance, (ii) angle stiffness, (iii) column/channel thickness and, (iv) presence of web angles.

2.2.1 Blind-bolted angle connections

As expected, *the deformation patterns* observed in blind-bolted connections subjected to pure tension arise from the behaviour of the individual connection components and their respective interactions. Figure 4 presents the deformation patterns observed for the four blind-bolted specimens. The interactions between the angle and Hollo-bolts as well as between the column flange and Hollo-bolts determine the inelastic mechanism that occurs. It can be observed from Figure 4 that plasticity occurred at the toe of the horizontal leg of the angle in specimens with gauge distance d=65 mm (Specimens T1 and T2 in Figures 4(a) and 4(b), respectively). Additionally, limited plastic deformation took place in the column flange when the thickness of the column was reduced from 10 mm in Specimen T1 to 6.3 mm in Specimen T2. On the other hand, large plastic deformations concentrated at the toe of the vertical angle when a shorter gauge distance was employed (d=40 mm) in Specimen T3 as shown in Figure 4(c). However, for Specimen T4 (Figure 4(d)) which incorporates a thinner column and stiffer angles, significant plastic deformations concentrated on the column flange which eventually lead to pull-out of the Hollo-bolts at a displacement of 22 mm. It can also be observed from Figure 4(d), that the 15 mm thick angle experienced very limited inelastic deformations. The tensile force-displacement relationships for the four Hollo-bolted specimens are depicted in Figure 5 together with an indication of their corresponding failure mechanisms. Figure 6 illustrates the development of plasticity in the left angles through measured strain values at selected locations.

The influence of *the angle horizontal gauge distance* (*d* in Figure 3) can be examined by comparing the results of specimens T1 and T3 with d=65 mm and d=40 mm, respectively. It can be observed from Table 3 and Figure 6 that the initial stiffness of Specimen T3 was 25% larger than that of Specimen T1 due to the shorter horizontal gauge distance (i.e. stiffer angle leg). Moreover, Specimen T3 developed 70% higher tensile yield forces than Specimen T1. However, Specimen T3 failed at a smaller displacement than Specimen T1 due to the fracture of the Hollo-bolt connecting the top angle and the column. It is important to note, with reference to Figures 4(a) and 4(c), that Specimen T1 also developed plasticity near the toe in the horizontal angle leg (column side). As for Specimen T3, most of the plastic deformation took place in the vertical angle leg (beam side). This can be further confirmed by observing the strain measurements depicted in Figures 6(b) and 6(c). As shown in Figure 6(b) plastic strains were reached first near the toe of the horizontal (column) angle leg in Specimen T1 (location S3 in Figure 6(a)), after which plastic strains developed at the toe of the vertical (beam) leg (location S2 in Figure 6(a)). With regards to Specimen T3 shown in Figure 6(c), yield strains were first reached near the toe of the vertical angle leg (location S2 in Figure 6(a)) followed by large plastic deformations. Plastic strain levels were also attained in the horizontal leg for connection displacements of over 8 mm in Specimen T3 (Figure 6(c)).

The *influence of column thickness* on the tensile behaviour of Hollo-bolted connections can be studied by comparing the results of specimens T1 and T2. The thickness of the column was reduced from 10 mm in Specimen T1 to 6.3 mm in Specimen T2, while all other geometric and

material characteristics were retained. It can be appreciated from Table 3 and Figure 5, that the initial stiffness of Specimen T1 was about 28% larger than that of Specimen T2 due to the thicker column. This level of difference is maintained up to the attainment of the connection yield capacity (i.e. 37 kN). After yielding, the tensile force-displacement responses for both specimens follow a similar path for displacements of up to 17 mm. Significant tension stiffening was observed in Specimen T1 owing to the concentration of plastic deformations in the angle components reaching failure at 47 mm of joint tensile displacement. While the ultimate capacity for Specimen T1 was 60 kN higher than that of Specimen T2, the development of significant plastic deformations in the column face of Specimen T2 delayed its failure up to a displacement of 53 mm, 7 mm higher than the failure displacement of Specimen T1.

As expected, the *stiffness of the column face* has a direct influence on the connection response. This can be observed by examining the behaviour of Specimen T4 where thick angles were used in combination with a column of 6.3 mm thickness. As expected, the reduction in the column wall thickness resulted in significant deformation around the Hollo-bolts in the thin column leading to a modest joint stiffness of around 38 kN/mm as shown in Table 3 and Figure 4. Moreover, a reduced connection ultimate capacity was observed (157 kN) caused by pulling-out of the Hollo-bolts connecting the angles and the column starting at a displacement of around 22 mm. Specimen T4 also had less ductility capacity in comparison with the other blind-bolted configurations (T1, T2 and T3).

2.2.2 Combined channel/angle connections

The main *deformation patterns* of the angle and channel components in the three combined channel/angle connection specimens tested are depicted in Figure 7. When a stiff angle (thickness = 15 mm and d = 45 mm) was combined with a thin channel component (thickness = 6.3 mm) in the case of Specimen T5 of Figure 7(a), the failure mechanism was governed by the deformation of the channel flange in bending with only minor plasticity occurring in the angle. Failure was reached at a load of 271 kN in Specimen T5 due to fracture around the bolt holes of the thin channel. On the other hand, in the case of Specimen T6 (shown in Figure 7(b)) with a 10 mm thickness channel, the tensile behaviour of the connection was dominated by the combination of bending deformations within the channel and angle. Specimen T6 reached an ultimate capacity of 380 kN at 33 mm when shear fracture of the standard bolts connecting the angle and beam flange occurred. On the other hand, Specimen T7 - which incorporates top, seat and web angle components - accumulated plastic deformations at the toe of the vertical leg (beam flange side) in top and seat as well as web angle components (Figure 7(c)). No signs of failure were evident at the end of test in Specimen T7 which exhausted the actuator force capacity at 700 kN. The tensile force-displacement relationships for Specimens T5, T6 and T7 are depicted in Figure 8 and the main response parameters are summarized in Table 3. These results are further discussed below in relation to the channel thickness and web angle contributions.

The *effect of reverse channel thickness* on the response of combined channel/angle connections can be examined by comparing the experimental results of Specimens T5 (with channel thickness =6.3 mm) and T6 (with channel thickness =10 mm). It can be observed from Table 3 and Figure 8 that the increase in channel thickness leads to a proportional increase in the stiffness and capacity which were about 40% and 55% higher for Specimen T6 in comparison with Specimen T5, respectively. Only minor plastic deformations were observed in the angle in Specimen T5 due to the concentration of plasticity in the face of the channel component at the early stage. On the other hand, some plasticity developed within the angles in Specimen T6 which incorporates a thicker channel. This can be further discussed with reference to the development of measured strains presented in Figures 9(b) and 9(c). It can be noted from Figure 9(c) that yield strain was reached at the toes of the angle legs (Locations S2 and S3) of Specimen T6 at an overall joint vertical displacement of around 10 mm. In contrast, the angle in Specimen T5 remained elastic up to 20 mm of vertical displacement (Location S2 and S3) in Figure 9(b). Moreover, Specimen T6 developed a plastic strain value of about 2.5% in the angle leg, which is 40% higher than the corresponding strains in Specimen T5 for equivalent joint displacements.

The response of bolted connection with *top and seat as well as web angles* subjected to tension load can be illustrated with reference to Specimen T7. As shown in Figure 7(c), the plastic deformation was concentrated in the angles, while minor plastic deformations were observed in the channel face. Importantly, the web angle configuration exhibited significantly higher stiffness and capacity when compared with the other top and seat details, as illustrated in Figure 8 and Table 3. The initial stiffness of Specimen T7 increased to 242 kN/mm, and the tensile force reached 700 kN (the actuator capacity) at a displacement of 29 mm.

2.3 Results and observations from compression tests

A total of three blind-bolted and three reverse channel connections were tested under compressive action, as depicted in Table 1. Table 4 summarizes the main response parameters of blind-bolted and reverse channel connections under compressive action, while Figures 10 to 13 present their respective deformation patterns and compression force-displacement relationships. The compression stiffness and yield capacity reported in Table 4 were obtained by means of a bilinear idealization considering a work conservation approach. The experimental results and observations are presented and discussed below. The tests were mainly designed in order to assess different beam/angle to column width ratios, as this was noted in previous studies [14] to be a key factor influencing the behaviour.

2.3.1 Blind-bolted angle connections

Figure 10 illustrates the deformation patterns of angles and columns for the three blind-bolted angle connections at the end of each test. Since the deformation for connection specimens under compressive force is symmetric, only the one angle and column side are represented in Figure 10. It is evident from the figure that plasticity took place at the column face in the area in direct contact with the beam flange. It is also evident from the figure that large plastic punching

deformations accumulated in the column face in the case of specimens with angle/beam widths smaller than the column face width (i.e Specimens C1 and C2). Significant flexural deformations also occurred in the horizontal (column) angle leg in these cases. On the other hand, when the width of the beam and angle exceeded that of the column face (Specimen C3 in Figure 10(c)), the plastic deformation was shared by the column lateral faces leading to a stiffer response.

The observed plastic deformation patterns have a direct influence on the resulting force-displacement relationships as illustrated in Figure 11. It is evident from the figure that the provision of beam/angle widths smaller than the corresponding column face width leads to proportional reductions in the connection stiffness and capacity. In the case of Specimen C1 (with column SHS 150x150x10) the initial stiffness was about 40% higher than that of Specimen C2 (with column SHS 200x200x10) for the same beam/angle width (i.e. 102 mm). Moreover, Specimen C1 yielded at a load about 140 kN higher than Specimen C2 and this difference increased to 180 kN for compressive capacities at 25 mm of displacement.

The effects of providing angle/beam components wider than the column face width can be illustrated by comparing the results of specimens C1 and C3 where the beam width is increased from 102mm in the former to 165 mm in the latter, while retaining all other geometric and material characteristics. This increment in the angle/beam width led to enhancements of around 70% and 55% in stiffness and capacity, respectively. The capacity of the connection under compression at 25 mm of compressive displacement also increased by 60% in Specimen C3 with respect to the corresponding capacity of Specimen C1.

2.3.2 Combined channel/angle connections

Three combined channel/angle connections were examined with emphasis on the influence of the stiffness of the reverse channel as well as the geometry and thickness of the angle components. The main deformation patterns of the three combined channel/angle connection specimens tested are depicted in Figure 12 while the corresponding compression force-displacement relationships are presented in Figure 13.

Notwithstanding the variation in the angle orientation and gauge distances between Specimens C4 and C5 (as illustrated in Table 1), only minor differences were observed between their overall *plastic deformation mechanisms* as can be noted from Figures 12(a) and 12(b). A similar deformation pattern was observed in both cases, where the inward deformation of the channel face reached its maximum value along the line of contact between the beam and column flanges while the top and seat angles deformed near the toe. Conversely, when thicker angles were combined with a thinner channel (as in Specimen C6), the plastic deformation concentrated in the channel flange, and the deformations in the angle components remained largely in the elastic range. Importantly, the deformation mode observed in the channel component of Specimen C6 was different to that observed in Specimens C4 and C5 in that significant punching deformations were developed along the full area of contact between the angle leg and column face (Figure 12).

The differences in deformation patterns noted above have a direct influence on the connection stiffness and yield capacity as shown in Figure 13. From this figure (and the values in Table 4) it can be observed that the stiffness of Specimen C4 was only 5% higher than that of Specimen C5 due to the slightly higher angle leg length. This is consistent with the similarities in the column face yield mechanism described before. Likewise, both Specimens C4 and C5 reached compressive capacities in the order of around 660 kN. In contrast, the thinner channel employed in Specimen C6 lead to a reduction of nearly 30% in stiffness and 50% in yield capacity when compared with the observed values for Specimens C4 and C5.

3. Numerical assessment

The experimental results and observations presented in this paper provide essential data for the validation of numerical and analytical models for semi-rigid angle connections to tubes. To this end, this section describes a detailed numerical model for blind bolted and reverse channel open beam-to-tubular column connections. The proposed continuum finite element models were developed in the general purpose program ABAQUS [22] and can offer a realistic simulation of the response of semi-rigid angle connections to tubes subjected to tension and compression actions. The model characteristics and validation studies are described below. These models are then used in subsequent sections of this paper to extend the experimental data-set with a view to proposing simplified expressions for the estimation of key connection design parameters such as stiffness and capacity.

3.1 Modelling details

Three-dimensional (3D) finite element models were developed using the FE software ABAQUS 6.7 [22]. These models make use of eight-node brick solid elements of Type C3D8I, as shown in Figure 14. Special attention was given to the faithful representation of the geometric and mechanical characteristics of the bolts including the shank, sleeve, head and nut, as illustrated in Figure 14. The stress-strain relationships for the material of all the connection components were defined by a tri-linear kinematic hardening rule with an elastic modulus of 210 GPa and Poisson's ratio 0.3. The models consider the experimentally obtained yield stress and ultimate strength values for the angle, beam and column components summarized in Table 2. The contact phenomena between each pair of interacting surfaces was taken into account by defining 'hard and friction' surface interaction properties. The more flexible surface was chosen as slave surface, while the more rigid area was assigned as master. Moreover, slippage between the bolt and hole surfaces was considered by means of standard ABAQUS contact definitions. To this end, a 'friction' surface was employed in the tangential direction with a friction coefficient of 0.3 [32]. Similarly, a 'hard' surface contact pressure over-closure relationship was defined in the normal direction to enforce no-overlapping between contact surfaces. Bolt pretension in standard and Hollo-bolts was introduced by means of two loading steps. Firstly, pretension forces of 110 kN for Grade 10.9 M16 bolts were applied, in accordance with the specified tightening torques. The second step involved removing the applied pretension force while simultaneously fixing the

bolt length at its deformed (shortened) value. The boundary conditions and loading in the numerical analyses followed the conditions and loading methods employed during the tests and described previously. Axial displacements were applied on a rigid plate tied to the end of the beam in the numerical models. A displacement control solution strategy was employed in all simulations with maximum displacements of 30 and 25 mm for tension and compression specimens, respectively. A number of mesh sensitivity studies were carried out in order to arrive at an optimum representation which involves a comparatively finer mesh for the angles and bolts as well as the areas within the beams and columns which are in contact with these components, whereas a relatively coarser mesh was employed elsewhere. The dimensions of the adopted mesh ranged between 6 mm within the refined region, and up to 100 mm within the coarser region. A more detailed account of the finite element models can be found elsewhere [32].

3.2 Numerical simulations

The comparisons between the experimental axial force-displacement relationships (obtained by means of the load cell and transducer incorporated within the actuator) and the corresponding FE predictions are presented in Figures 15 and 16 for the tension and compression tests, respectively. It is evident from the plots in Figure 15 that the FE models provide a good prediction of the experimental tensile behaviour in all cases. The initial stiffness, yield displacement and post-yield response match reasonably well the experimental behaviour. In the case of Specimens T3, T6 and T7, the yield forces are overestimated by the numerical predictions within a range of 20%. These discrepancies can be related to the difficulties of modelling the local rotational behaviour of the bolts connecting the column/channel and the angle; this has a more pronounced effect as the vertical gauge distance in the angle decreases such as in the case of Specimens T3, T6 and T7 (where d =40 mm) as opposed to Specimens T1 and T2 where a larger distance is employed (d=65 mm). Some minor differences are evident in the case of Specimens T1-T4 and T6, where slippage occurs almost instantaneously once the friction forces are overcome in the FE simulations whereas a more gradual slip displacement is observed in the tests. In the case of Specimen T4 (Figure 15(d)), the numerically obtained forces closely resemble the experimental values up to about 7 mm. At a displacement of around 7mm, the Hollo-bolt clamping action was overcome in the FE model and the blind-bolt started to pull out leading to a decrease in the predicted tension force which reached a local minimum of 110 kN at a displacement of around 13 mm. However, this phenomenon did not occur during the test. This discrepancy can be attributed to uncertainties in the sleeve material properties assumed and the highly localized effects in the Hollo-bolt/column face interaction zone. Likewise, during the test, inside deformations within the legs of the Hollo-bolt sleeve resulted in complete pull out of the Hollo-bolts at a displacement of 23 mm. Nevertheless, this phenomenon is not captured by the FE model leading to the discrepancies observed after 20 mm of tensile displacement as indicated in Figure 15(d).

Figure 16 presents comparisons of the compressive force-displacement relationships between experimental results and numerical predictions. Close correlation is observed in terms of

stiffness, capacity and post-elastic response for all specimens. In the case of Specimens C1, C2, C3 and C6, minor discrepancies arise after a displacement of around 1 mm due to hardening of the initial stiffness in the numerical model which can be attributed to gap closure. Minor geometric imperfections may have prevented these hardening effects during testing of the actual specimens. In general, this good agreement between the FE simulations and the test results shows that the detailed FE model can capture the response of blind bolted as well as reverse channel angle connections in compression.

Having gained confidence in the reliability of the detailed FE model, this is used in subsequent sections of this paper to complement and validate the formulation of component-based expressions for the prediction of the axial response of semi-rigid connections to tubes.

4. Component characterization

In general, any typical connection configuration can be idealised as an assemblage of uniaxial springs following the well-established component-based method [4, 33]. This section evaluates existing component representations and proposes new expressions for the estimation of the axial stiffness and capacity of key connection elements. These component characteristics are then employed in the subsequent section to assemble the full connection response.

4.1 Channel face in tension

The *tensile resistance* of reverse channel component for a two-bolt arrangement, F_{cft}, can be determined from the bolt force equation proposed by Málaga-Chuquitaype and Elghazouli [16] as:

$$F_{cft} = f_{y,c} {t_c}^2 \left(\frac{2R_m - d_0}{2R_m - d_{bh}}\right)\left[\pi \frac{d_0 - R_m}{d_0 - 2R_m} + 2\frac{i + 2c - d_0}{2R_m - d_0}\right] \qquad (1)$$

where R_m represents:

$$R_m = \frac{b_c - t_c - i}{2} \qquad (2)$$

in which b_c is the width of the channel, t_c is the thickness of the channel, $f_{y,c}$ is the yield stress of the channel, i is the bolt pitch dimension (as depicted in Figure 3), d_0 is the hole diameter, and d_{bh} is the bolt head diameter.

Similarly, the *initial stiffness* of the channel face with a two-bolt arrangement can be evaluated by [28]:

$$K_{cft} = \frac{\pi E {t_c}^3}{6(1 - \upsilon^2) C_t \left(\frac{b_c - t_c}{2}\right)^2} \qquad (3)$$

where E is the Young's Modulus of the steel, υ the Poisson's ratio for steel and C_t is a coefficient which is related to the bolt arrangement.

Figure 17 depicts the variation of C_t as a function of the ratio i/m_c (Figure 17(a)) and as a function of the dimension L (Figure 17(b)) where L represents the distance from the bolt centre line to the free end of the reverse channel, i is the bolt pitch and m_c is defined as:

$$m_c = \frac{b_c - 2t_c - 2r_c}{2} \tag{4}$$

where r_c is the column root radius.

Trend lines obtained from least square regression analyses and their corresponding correlation coefficients (R) are also presented in Figure 17. The data-base portrayed in Figure 17 was obtained from extensive calibration studies using the detailed FE models described in the previous section. Column segments of varying length with symmetric boundary conditions were employed as illustrated in Figure 18(a). An evenly distributed axial load was applied over the angle area in direct contact with the bolt head. Optimal values of C_t were then obtained as those that would minimize the differences between the stiffness estimations of Equation 3 and the FE predictions. Two clearly distinguishable behavioural regions were identified as shown in Figure 17: (i) a region in which the distance from the bolt centre line to the free end of the reverse channel (i.e. L in Figure 18(b)) has a direct influence on the channel component stiffness and (ii) a region in which the distance L no longer affects the channel initial stiffness. A value of L = 100 mm was considered suitable to demarcate the two behavioural regions. Therefore, a general equation for the determination of the value of C_t can be defined as:

$$C_t = Q_t \cdot \left(0.24e^{-0.3i/m_c}\right) \tag{5}$$

where,

$$Q_t = \begin{cases} 6L^{-0.4} & if\ L < 100mm \\ 1 & if\ L \geq 100mm \end{cases} \tag{6}$$

4.2 Column face in tension

The *tensile resistance* of the column face can be calculated from Equations 7 to 11 as proposed by Gomez [34-35]. In these expressions the tensile capacity of the column flange is taken as the minimum value of the local yielding force, $F_{cft,1}$, and the punching resistance, $F_{cft,2}$, thus:

$$F_{cft} = min\left(F_{cft,1}, F_{cft,2}\right) \tag{7}$$

where

$$F_{cft,1} = \begin{cases} \dfrac{n_b \pi d_0 t_c f_{y,c}}{\sqrt{3}} & if \quad 2(i+0.9d_0) > n_b \pi d_0 \\ \dfrac{2(i+0.9d_0) t_c f_{y,c}}{\sqrt{3}} & if \quad 2(i+0.9d_0) < n_b \pi d_0 \end{cases} \tag{8}$$

and

$$F_{cft,2} = \delta \varepsilon \frac{{t_c}^2 f_{y,c}}{4} \tag{9}$$

where n_b is the number of bolts in the column face, and the factors δ and ε are calculated from Equations 10 and 11 below:

$$\delta = \frac{4}{1-\frac{i}{b_c}} \left(\pi \sqrt{1-\frac{i}{b_c}} \right) + 2\frac{0.9d_0}{b_c} \tag{10}$$

$$\varepsilon = \begin{cases} 1 & if \ \dfrac{i+0.9d_0}{b_c} > 0.5 \\ 0.7 + \dfrac{0.6(i+0.9d_0)}{b_c} & if \ \dfrac{i+0.9d_0}{b_c} < 0.5 \end{cases} \tag{11}$$

Additionally, *the tensile stiffness* of the column face component in Hollo-bolted connections can be estimated through Equations 3 and 5 by assuming a distance of L>100 mm.

4.3 Angle/bolt assemblage in tension

The *tensile resistance* of the bolted angle in tension, F_{at}, can be determined [16] by means of the equivalent T-stub procedure suggested in Eurocode 3 Part 1.8 [4], therefore:

$$F_{at} = \min\left(F_{at,1}; F_{at,2}; F_{at,3}\right) \tag{12}$$

where the minimum value of three possible failure modes is considered as follows:

Mode 1, in which a plastic mechanism forms in the angle:

$$F_{at,1} = \frac{4M_{pl}}{d'} \tag{13}$$

Mode 2, that considers a mixed failure mode involving yielding of the bolt and a plastic hinge in the angle:

$$F_{at,2} = \frac{2M_{pl} + c' \sum F_{bt}}{d' + c'} \tag{14}$$

Mode 3, in which yielding of the bolts occur:

$$F_{at,3} = \sum F_{bt} \tag{15}$$

with

$$M_{pl} = 0.25 b_{eff} t_a^{\,2} f_{y,a} \tag{16}$$

Where $f_{y,a}$ is the yield stress of angle, b_{eff} is the effective width of the angle taken as half of the angle width b_a, F_{bt} is the bolt capacity, and the distances c' and d' are the effective gauge distances considering the influence of the angle stiffness on the location of the plastic hinges defined by Málaga-Chuquitaye and Elghazouli [28] as:

$$c' = c + (1 - f_{pry})\frac{d_b}{2} \leq 1.25(d - 0.8r_a - t_a) \tag{17}$$

$$d' = d - 0.8r_a - t_a - (1 - f_{pry})\frac{d_b}{2} \tag{18}$$

where dimensions c and d are the nominal gauge distances depicted in Figure 3, t_a is the angle thickness, r_a is the angle root radius, d_b is the bolt diameter and f_{pry} is a factor that takes into account the change in the location of the plastic hinge and which is related to the ratio of the stiffness of the bolt and the stiffness of the angle component. The factor f_{pry} can be taken as 1 when $k_b \leq 3(d - 0.8r_a - t_a)^3/EI$ and 0 when $k_b \geq 12(d - 0.8r_a - t_a)^3/EI$ in which k_b is the stiffness of the bolt and I is moment of inertia of the angle section. A linear interpolation between these limits can be employed for the cases:

$$12(d - 0.8r_a - t_a)^3/EI > k_b > 3(d - 0.8r_a - t_a)^3/EI.$$

In the case of combined channel/angle connections, where standard bolts are used to connect the angle to the reverse channel, the bolt tensile capacity, F_{bt} in Equations 14 and 15, can be determined from [4]:

$$F_{st} = f_{u.b} A_s \tag{19}$$

where $f_{u.b}$ is the ultimate stress of the bolt and A_s its cross sectional area. On the other hand, if M16 Hollo-bolts are employed, the bolt tensile capacity (F_{bt} in Equations 14 and 15) can be assumed to be 78 kN or 32 kN for Grade 10.9 or Grade 8.8 bolts, respectively [14].

Additionally, the stiffness of the angle/bolt assemblage in tension can be determined from the contribution of the bending stiffness of the angle and the axial stiffness of the bolt acting in series as follows:

$$K_{abt} = \frac{1}{\frac{1}{K_{at}} + \frac{1}{K_{bt}}} \quad (20)$$

The following equation can be employed for the estimation of the bending stiffness of the angle component, K_{at} [4]:

$$K_{at} = \frac{E b_{eff} {t_a}^3}{d'^3} \quad (21)$$

Similarly, the Hollo-bolt stiffness K_{ht} can be assumed to be 195 kN/mm or 160 kN/mm for Grade 10.9 or 8.8 bolts, respectively [14]. On the other hand, the initial stiffness of standard bolts, K_{st}, is given by [4]:

$$K_{st} = 1.6 \frac{E A_s}{L_b} \quad (22)$$

where L_b is the bolt elongation length, taken as the grip length (total thickness of material and washers), plus half the sum of the height of the bolt head and the height of the nut, and A_s is the bolt cross sectional area.

4.4 Channel/angle assemblage in compression

As noted previously, the interaction between the angle and reverse channel components has a direct influence on the development of the compressive inelastic mechanism of the connection. Accordingly, both components are treated jointly herein and the compressive yield capacity of the connection is determined from the deformation pattern with minimum required energy over the full range of possible channel/angle assemblage mechanisms. To this end, two main plastic deformation patterns were identified from the experimental study described above, as illustrated in Figures 19 and 20. Mechanism 1 (of Figure 19(a)) forms when the relative stiffness of the angle component allows it to deform inwards in the direction of the compression load. In this mechanism, lines DR, RE, EG, GS, SF and FD are assumed to have zero vertical displacement, while Lines HI, IJ, JH, JM, ML, LK and KM are assumed to displace vertically by the same amount. Accordingly, the distances y and z can be obtained as a function of x (Figure 19(a)):

$$y = \frac{B(C - B)}{4x} \quad (23)$$

$$z = \frac{C}{B} x \quad (24)$$

where C is calculated from:

$$C = b_c - t_c \quad (25)$$

and B can be evaluated from Equation 26 below depending on the beam-to-column width ratio as:

$$B = \begin{cases} \min(b_a; b_b) & if\ b_c \leq \min(b_a; b_b) \\ b_c - 2t_c - 2r_c & if\ b_c > \min(b_a; b_b) \end{cases} \quad (26)$$

where, b_c is the width of the channel, b_b the width of the beam, b_a the width of the angle. and h is the height of the beam.

Based on these idealisations, the plastic capacity of the channel in compression F_{cfc} under Mechanism 1 can be derived as:

$$F_{cfc,1} = 2 \cdot f_{y,c} {t_c}^2 \left[\sqrt{\frac{C+3B}{C-B}} + \sqrt{\frac{2B}{C-B}} + \frac{h}{C} \right] \quad (27)$$

where

$$A = \frac{\sqrt{(C+3B)\cdot(C-B)}}{2} \quad (28)$$

$$x = \frac{B}{C}\sqrt{\frac{B(C-B)}{2}} \quad (29)$$

Additionally, the inward deformation of the angle component can follow one of the two possible patterns depicted in Figure 19(b) depending on the length of the angle leg. Therefore, the plastic capacity of the angle in compression $F_{ac,1}$ can be derived as:

$$F_{ac} = \begin{cases} 1.5 \cdot f_{y,a} {t_a}^2 \left[\frac{B}{A}\right] & if\ A > L_a \\ 0.5 \cdot f_{y,a} {t_a}^2 \left[\frac{B}{A} \cdot \left(1 + \frac{L_a}{A}\right)\right] & if\ A \leq L_a \end{cases} \quad (30)$$

Where L_a is the distance between beam flange and the angle edge in mm.

An alternative yield mechanism, Mechanism 2, is that depicted in Figure 20. This will form when the angle is relatively stiff so as to prevent the occurrence of yielding in any of its legs. This mechanism assumes that the vertical displacement of Lines DF and EG in Figure 20 is zero. Similarly, the vertical displacements of Lines RH, HJ, TI, JM, ML, MK, LU and KS are assumed to be equal. The length of Lines RH and TI is assumed to be L_c (the distance between beam flange and channel edge). Consequently, the channel/angle yield resistance of Mechanism 2 can be evaluated from:

$$F_{cfc,2} = 2 \cdot f_{y,c} t_c^{\,2} \left[\frac{2L_c}{C-B} + \sqrt{2}\frac{B}{C} + \frac{h}{C} \right] \quad (31)$$

Therefore, the capacity of the channel/angle assemblage in compression, F_c, can be determined as:

$$F_c = min\left[\left(F_{cfc,1} + F_{ac} \right); \left(F_{cfc,2} \right) \right] \quad (32)$$

In addition, the stiffness of the channel in compression, K_{cfc}, can be determined through the relationship proposed by Malaga-Chuquitaype and Elghazouli [28] for the initial stiffness of Hollow-section faces as follows:

$$K_{cfc} = \frac{\pi E t_c^{\,3}}{6(1-\upsilon^2) C_c \left(\frac{b_c - t_c}{2} \right)^2} \quad (33)$$

where the coefficient C_c is an empirical coefficient defined with reference to Figure 21. Figure 21(a) presents the FE model employed for the determination of C_c. A channel face was modelled in ABAQUS and subjected to a distributed compressive load applied through the angle component. Figure 21(b) presents the values of C_c as a function of the ratio between the column width, C, and beam width, B. The influence of the distance between the beam flange and the channel edge, L_c, is also illustrated in Figure 21(c). Using curve fitting, the general equation for the determination of C_c can be defined as:

$$C_c = Qc \cdot (0.3\ln(C/B) + 0.03) \quad (34)$$

where Q_c is taken as 1 when L_c >100 mm, while Q_c is obtained as $7L_c^{(-0.4)}$ from Figure 21(c) when L_c ≤100 mm.

The stiffness of the angle leg (beam side) in compression can be estimated as:

$$K_{ac} = \frac{n_b' E d_0 t_a}{a} \quad (35)$$

Where n_b' is the number of the bolts in the angle leg and the distance a is defined in Figure 3. Finally, the stiffness of the channel/angle assemblage in compression, K_c, can be determined from the contribution of the stiffness of the channel and the angle:

$$K_c = \frac{2}{\frac{1}{K_{cfc}} + \frac{1}{K_{ac}} + \frac{1}{K_{bs}}} \quad (36)$$

where K_{bs} is the stiffness of the bolts in shear. Equation 36 accounts for the presence of top and seat angle components

4.5 Column/angle assemblage in compression

The response of the column and angle components under compression can be also characterized by Mechanism 1 shown in Figure 19. Therefore, the compressive resistance of the column face can be evaluated by Equation 27. Similarly, Equation 30 can also be employed for the estimation of the angle capacity in compression. Hence, the capacity of the column/angle assemblage in compression F_c is:

$$F_c = F_{cfc,1} + F_{ac} \tag{37}$$

On the other hand, Equation 36 can be employed to estimate the stiffness of the column/angle assemblage in compression.

5. Prediction of connection response

The observations and component characterizations presented previously are used herein to propose simplified expressions suitable for practical connection design. In particular, expressions for the evaluation of the connection stiffness and capacity under direct axial action are presented.

5.1 Tensile behaviour

Based on the simplified component model characterization presented above, the design value of the connection tensile resistance, F_t, can be determined as:

$$F_t = \sum_{i=1}^{n_r} F_{it} \tag{38}$$

with

$$F_{it} = \min(F_{cft}; F_{at}; F_{bs}; F_{ab}; F_{bb}) \tag{39}$$

where F_{it} is the tensile resistance of the i-th bolt row, n_r is the number of the bolt rows in tension, F_{cfc}, F_{at}, F_{bs}, are the resistance of column/channel face in tension, bolted angle in bending (including the effect of the bolts in tension) and bolt in shear for the i-th bolt row, respectively. Additionally, the bearing resistance of the angle leg (F_{ab}) and beam flange (F_{bb}) are considered in Equation 39. These can be evaluated by the corresponding expressions for plate bearing proposed in Eurocode 3 [4].

Also, the overall joint stiffness can be evaluated as:

$$K_t = \sum_{i=1}^{n_r} K_{it} \tag{40}$$

with

$$K_{it} = \frac{1}{\frac{1}{K_{cft}} + \frac{1}{K_{abt}} + \frac{1}{K_{bs}} + \frac{1}{K_{ab}} + \frac{1}{K_{bb}}} \tag{41}$$

where K_{it} is the tensile stiffness of the i-th bolt row, n_r is the number of the bolt rows in tension, and K_{cfc}, K_{abt}, K_{bs}, K_{ab} and K_{bb} are the initial stiffness of column/channel face in tension, angle/bolt assemblage in tension, bolt in shear, angle leg in bearing and beam flange in bearing for the i-th bolt row, respectively. The initial stiffness of the angle leg (K_{ab}) and beam flange (K_{bb}) in bearing can be estimated from the corresponding equations proposed in Eurocode 3 [4] for plate bearing stiffness.

5.2 Compressive behaviour

As noted previously, the interaction between the angle and channel/column face determines the deformation pattern and yield mechanism observed in the connection. To this end, Sections 4.4 and 4.5 characterized the joint action of both channel and angle components under compression. Therefore, Equations 32 and 37 are used herein for the evaluation of the overall connection compression resistance. Similarly, Equation 36 is employed to examine the stiffness characteristics of the connections.

5.3 Comparative assessment

The simplified model proposed above is validated herein against the results of the tests described in Section 2. Figure 22 presents the comparisons in terms of tensile force-displacement relationships, whilst Figure 23 presents the corresponding compression force-displacement curves. It should be noted that no assumptions were made regarding the post-elastic stage within the component-based approach and thus the force-displacement curves depict an elastic-perfectly plastic idealization. Nevertheless, it is clear from Figures 22 and 23 that the suggested simplified model provides a reasonably good estimation of the initial stiffness and yield capacity in nearly all cases, as discussed below.

As demonstrated in Figure 22, the initial stiffness based on the component response match the experimental results well within an accuracy of ±5% for all tensile specimens except Specimen T4. The differences observed for Specimen T4 can be attributed to be the idealization of the Hollo-bolt in tension. In this test, the extremely stiff angle employed resulted in pulling-out of the Hollo-bolt and caused complex local interactions as explained before.

Figure 23 compares the compressive force-displacement response between the proposed simplified model and the respective test results. As in the case of tension action, it is evident from Figure 23 that the simplified model provides a close prediction of the connection compressive response including the initial stiffness and yield capacity. In general, it is shown that the simplified model can capture the main features of the connection response subjected to compressive action.

6. Conclusion

The behaviour of bolted angle connections between tubular columns and open beams under axial force has been examined by means of experimental and numerical studies as well as simplified analytical models. An experimental programme comprising seven tensile tests and six compressive tests on blind-bolted angle connections and combined channel/angle configurations has been described in detail. The main behavioural patterns were identified, and the key response characteristics such as stiffness, capacity and failure mechanism were discussed. The experimental results also provided necessary information for the validation and calibration of complementary finite element and simplified analytical models.

The inelastic mechanisms exhibited by Hollo-bolted connections under tensile force were identified. These mechanisms primarily originate from the interaction between the angle components and Hollo-bolt/column face assemblage. It was shown that the angle gauge distance, between column bolt centre and beam flange, has a significant effect on the initial stiffness and tensile capacity of the connection. Besides, the thickness of the column also has a notable influence on the connection capacity, in particular when thicker angles are employed. The tests also showed that a reduction of the column thickness can lead to considerable reduction in the joint stiffness and to the accumulation of plastic deformations around the Hollo-bolts which should be limited in design in order to satisfy serviceability requirements.

In addition, the inelastic mechanisms exhibited by combined channel/angle connections in tension were identified. As with blind-bolted connections, these inelastic patterns stem directly from the interaction between different connection components. For stiffer angles, the thickness of the reverse channel stands in direct relationship to the connection capacity and stiffness. Furthermore, the addition of web angles was shown to significantly enhance the overall connection tensile resistance.

In the case of Hollo-bolted connections subjected to compression, the inelastic mechanisms were largely determined by the relative widths of the column and the beam/angle components. Large plastic deformations accumulated in the column face in the case of specimens with angle/beam widths smaller than the column face width. Conversely, plastic deformation involved the column lateral faces when the width of the beam and angle exceeded that of the column face. Moreover, the provision of beam/angle widths smaller than the corresponding column faces lead to proportional reductions in the connection stiffness and capacity. As with blind-bolted

connections, the importance of ensuring an adequate mechanism for transferring the compression forces to the channel component has been highlighted. The main deformation patterns of combined channel/angle connections under compressions were also identified. The flexibility of the reverse channel component relative to the stiffness of the angles was shown to have a direct influence on both the initial stiffness and capacity of the connection.

A three-dimensional finite element model was developed to simulate the response of bolted angle beam-to-tubular column connections subjected to direct tension and compression actions. Results obtained by means of this FE representation were compared with the experimental response in order to assess the accuracy of the numerical model in terms of connection stiffness, capacity and failure mode. In general, the FE estimations were found to correlate well with experimental results in the pre-yielding and yielding range and up to large levels of displacement demands. This good agreement between the FE simulations and the test results show that the proposed FE models can capture the actual response of blind bolted as well as reverse channel angle connections.

Expressions for the estimation of connection stiffness and capacity under axial action have been proposed and validated. To this end, new component characteristics have been suggested for the column face in tension, column face in compression as well as the angle in tension and angle in compression. These expressions were found to produce reliable estimates of Hollo-bolted and combined channel/angle connection stiffness and capacities for the configurations considered in this investigation.

Acknowledgements

The support of Tata Steel Tubes for the research described in this paper is gratefully acknowledged. The authors are also grateful to the technical staff of the Structures Laboratories at Imperial College London, particularly Mr T. Stickland and Mr R. Millward, for their assistance with the experimental work. Additionally, the first author would like to acknowledge the grant provided by The China Scholarship Council and The UK Department for Innovation, Universities & Skills for her doctoral research studies through a UK/China Scholarship for Excellence.

References

1. Kukreti AR, Murray TM, Abolmaali A. End-Plate Connection Moment Rotation Relationship. *Journal of Constructional Steel Research* 1987. 8: 137-157.
2. Shen J, Astaneh-Asl A. Hysteretic behavior of bolted-angle connections. *Journal of Constructional Steel Research* 1999. 51(3): 201-218.
3. Garlock M, Ricles J, Sause R. Cyclic load tests and analysis of bolted top and seat angle connection. *Journal of Structural Engineering-ASCE* 2003. 129(12): 1615-1625.
4. CEN.EN1993-1-8. Eurocode 3: Design of steel structures, Part 1-8: Design of joints. Vol. 1-8, 1998.

5. Banks G. Flowdrilling for tubular structures, in *Proceedings of the Fifth International Symposium on Tubular Structures*, UK, 1993.
6. Ballerini M, Piazza M, Bozzo E, Occhi F. Shear capacity of blind bolted connections for RHS steel structural elements, in *Proceedings of the seventh international symposium on tubular structures*, Hungary, 1996.
7. France JE, Buick Davison J, Kirby PA. Strength and rotational stiffness of simple connections to tubular columns using flowdrill connectors. *Journal of Constructional Steel Research* 1999. 50(1): 15-34.
8. Huck International Inc. Industrial fastening system. Arizona (USA), 1990.
9. Korol R. Blind bolting W-shape beam to HSS columns. *Journal of Structural Engineering-ASCE* 1999. 119(12): 3463-3481.
10. Klippel S. Recent design developments with blind mechanically operated bolt systems for use with hollow section steelwork. *Journal of Constructional Steel Research* 1998. 46(1): 267-268.
11. Lindapter International Ltd. Type HB hollo-bolt for blind connection to structural steel and structural tubes. Lindapter International Ltd, UK, 1995.
12. Barnett T, Tizani W, Nethercot D. The practice of blind bolting connections to structural hollow sections: A review. *Steel and Composite Structures* 2001. 1(1): 1-16.
13. Barnett T, Tizani W, Nethercot D. Blind bolted moment resisting connections to structural hollow sections, in *Connections in Steel Structures IV*. Virginia, USA, 2000.
14. Elghazouli AY, Málaga-Chuquitaype C, Castro JM, Orton AH. Experimental monotonic and cyclic behaviour of blind-bolted angle connections. *Engineering Structures* 2009. 31(11): 2540-2553.
15. Ding J, Wang YC. Experimental study of structural fire behaviour of steel beam to concrete filled tubular column assemblies with different types of joints. *Engineering Structures* 2007. 29(12): 3485-3502.
16. Málaga-Chuquitaype C, Elghazouli AY. Behaviour of combined channel/angle connections to tubular columns under monotonic and cyclic loading. *Engineering Structures* 2010. 32(6): 1600-1616.
17. Krishnamurthy N, Graddy DE. Correlation between 2- and 3-dimensional finite element analysis of steel bolted end-plate connections. *Computers & Structures* 1976. 6(4-5): 381-389.
18. Citipitioglu AM, Haj-Ali RM, White DW. Refined 3D finite element modeling of partially-restrained connections including slip. *Journal of Constructional Steel Research* 2002. 58(5-8): 995-1013.
19. Kishi N, Ahmed A, Yabuki N, Chen WF. Nonlinear finite element analysis of top and seat-angle with double web-angle connections. *Structural Engineering and Mechanics* 2001. 12(2): 201-214.
20. Pirmoz A, Daryan AS, Mazaheri A, Darbandi HE. Behavior of bolted angle connections subjected to combined shear force and moment. *Journal of Constructional Steel Research* 2008. 64(4): 436-446.
21. Pirmoz A, Khoei AS, Mohammadrezapour E, Daryan AS. Moment-rotation behavior of bolted top-seat angle connections. *Journal of Constructional Steel Research* 2009. 65(4): 973-984.
22. ABAQUS. ABAQUS Theory Manual,Version 6.7. Hibbit, Karlsson and Sorensen Inc., 2003.

23. Wang ZY, Tizani W, Wang QY. Strength and initial stiffness of a blind-bolt connection based on the T-stub model. *Engineering Structures* 2010. 32(9): 2505-2517.
24. ANSYS. ANSYS Multiphisics 10.0. Canonsbury, Pennsylvania Inc, 2003.
25. Kishi N, Chen WF. Moment-rotation relations of semi-rigid connections with angles. *Journal of Structural Engineering* 1990. 116(7): 1813-1834.
26. Angerskov H. High strength bolted connections subjected to prying. *Journal of the Structural Division-ASCE* 1976. 102(1): 161-175.
27. De Stefano M, De Luca A, Astaneh Asl A. Modeling of cyclic moment-rotationresponse of double-angle connections. *Journal of Structural Engineering* 1994. 120(1): 212-229.
28. Málaga-Chuquitaype C, Elghazouli AY. Component-based mechanical models for blind-bolted angle connections. *Engineering Structures* 2010. 32(10): 3048-3067.
29. Ghobarah A, Mourad S, Korol RM. Moment-rotation relationship of blind bolted connections for HSS columns. *Journal of Constructional Steel Research* 1996. 40(1): 63-91.
30. Málaga-Chuquitaype C. Seismic behaviour and design of steel frames incorporating tubular members. PhD thesis, Department of Civil and Environmental Engineering, Imperial College London, UK, 2011.
31. Vlassis AG, Izzuddin BA, Elghazouli AY, Nethercot DA. Progressive collapse of multi-storey buildings due to sudden column loss-Part II: Application. *Engineering Structures* 2008. 30(5): 1424-1438.
32. Liu Y. Behaviour of steel connections under extreme loading conditions. PhD Thesis, Department of Civil and Environmental Engineering, Imperial College London, UK, 2012.
33. Faella C, Piluso V, Rizzano G. Structural Steel Semi-Rigid Connections: Theory, Design and Software. Florida, USA: CRC Press, 2000.
34. Gomes FCT. Etat limite ultime de la résistance de l'ame d'une colonne dans un assemblage semi-rigide d'axe faible. *Rapport interne 203, Technical Report, University of Liege* 1990.
35. Gomes FCT. Moment capacity of beam-to-column minoraxis joints, in *Proceedings of IABSE International Colloquium on Semi-Rigid Structural Connections*, Istanbul, Turkey, IABSE.319-326, 1996.

Tables

Table 1: Summary of the test specimens

Reference	Type	Column	Beam	Angle	Channel	Dimensions (mm) (as shown in Figure 3)											
						a	b	c	d	e	f	g	h	i	j	k	l
Tension tests																	
Blind-bolted angle connections																	
T1	A	SHS 150×150×10	UB 305×102×25	L100×75×8	-	45	30	35	65	-	-	-	100	45	45	-	-
T2	A	SHS 150×150×6.3	UB 305×102×25	L100×75×8	-	45	30	35	65	-	-	-	100	45	45	-	-
T3	A	SHS 150×150×10	UB 305×102×25	L100×75×8	-	50	50	35	40	-	-	-	100	45	45	-	-
T4	A	SHS 150×150×6.3	UB 305×102×25	L100×80×15	-	50	100	35	45	-	-	-	100	45	45	-	-
Combined channel/angle connections																	
T5	B	SHS 200×200×10	UB 305×102×25	L100×80×15	SHS 150×150×6.3	50	100	35	45	-	-	-	100	45	45	475	70
T6	B	SHS 200×200×10	UB 305×102×25	L100×80×15	SHS 150×150×10	50	100	35	45	-	-	-	100	45	45	475	70
T7	C	SHS 200×200×10	UB 305×165×25	L100×75×8	SHS 150×150×10	50	50	35	40	35	95	12.5	100	80	45	465	70
Compression tests																	
Blind-bolted angle connections																	
C1	A	SHS 150×150×10	UB 305×102×25	L100×75×8	-	50	50	35	40	-	-	-	100	45	45	-	-
C2	A	SHS 200×200×10	UB 305×102×25	L100×75×8	-	50	50	35	40	-	-	-	100	45	45	-	-
C3	A	SHS 150×150×10	UB 305×165×40	L100×75×8	-	50	50	35	40	-	-	-	150	45	45	-	-
Combined channel/angle connections																	
C4	B	SHS 200×200×10	UB 305×102×25	L100×75×8	SHS 150×75×10	45	30	35	65	-	-	-	100	45	45	515	70
C5	B	SHS 200×200×10	UB 305×102×25	L100×75×8	SHS 150×75×10	50	50	35	40	-	-	-	100	45	45	465	70
C6	B	SHS 200×200×10	UB 305×102×25	L100×80×15	SHS 150×75×6.3	50	100	35	45	-	-	-	100	45	45	475	70

Table 2: Material properties of connection components

	Yield stress (N/mm^2)	Ultimate stress (N/mm^2)
UB 305×165×25	329	443
UB 305×102×25	400	490
SHS 200×200×10	433	487
SHS 150×150×10	334	433
SHS 150×150×6.3	385	485
L 100×75×8	312	438
L 100×80×15	293	449
Hollo-bolt sleeve*	382	512

*Obtained from the mean of three hardness tests

Table 3: Summary of results for tensile tests

Reference	Initial stiffness (kN/mm)	Yield force (kN)	Failure	
			Force (kN)	Displacement (mm)
T1	79	37	231	46
T2	57	71	171	53
T3	105	135	310	38
T4	38	111	157	22
T5	95	94	271	32
T6	163	209	380	33
T7	242	285	-	-

Table 4: Summary of results for Compressive tests

Reference	Initial stiffness (kN/mm)	Yield force (kN)	Force (kN) at a displacement of 25 mm
C1	236	575	795
C2	136	433	610
C3	400	889	1211
C4	207	656	885
C5	193	672	825
C6	127	337	417

Figures

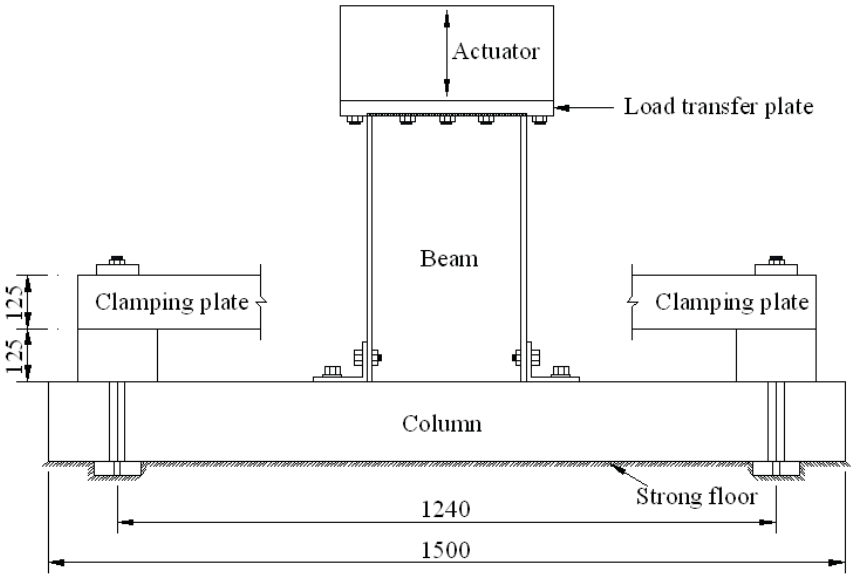

(a) Lateral view

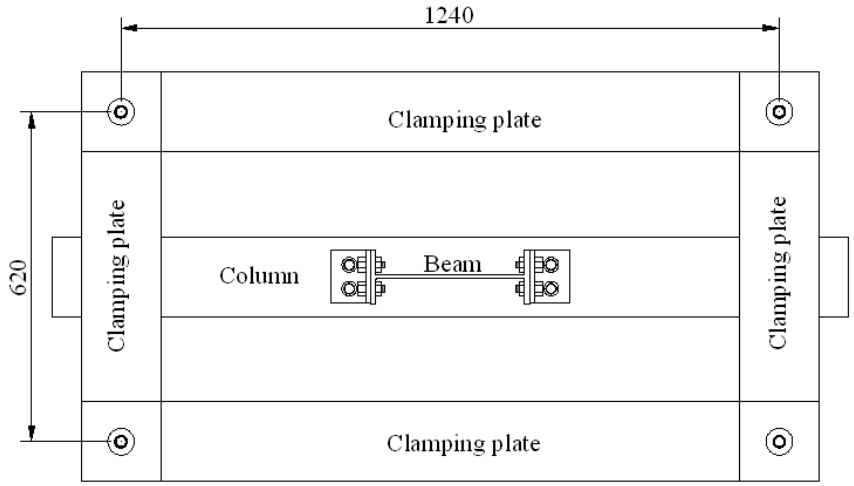

(b) Plane View

Figure 1: Tension test set-up (dimensions in mm)

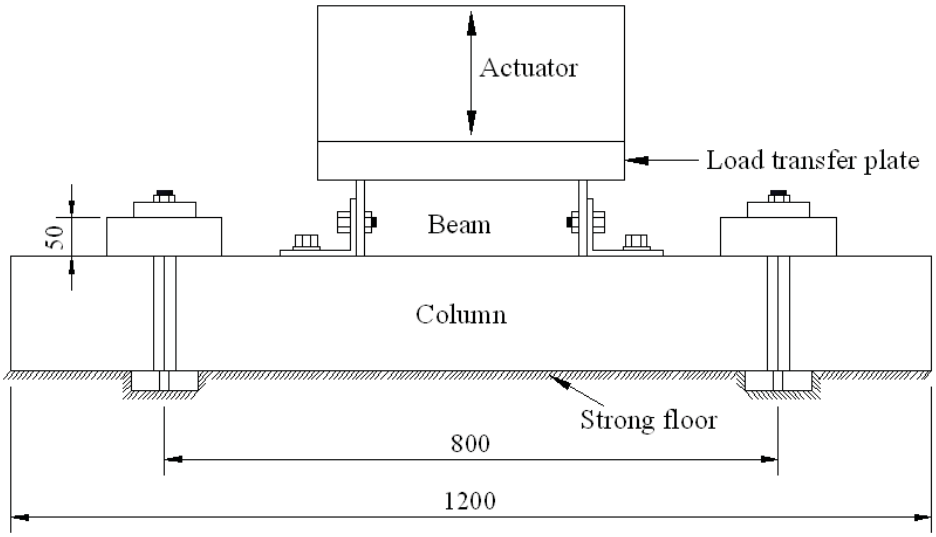

(a) Lateral view

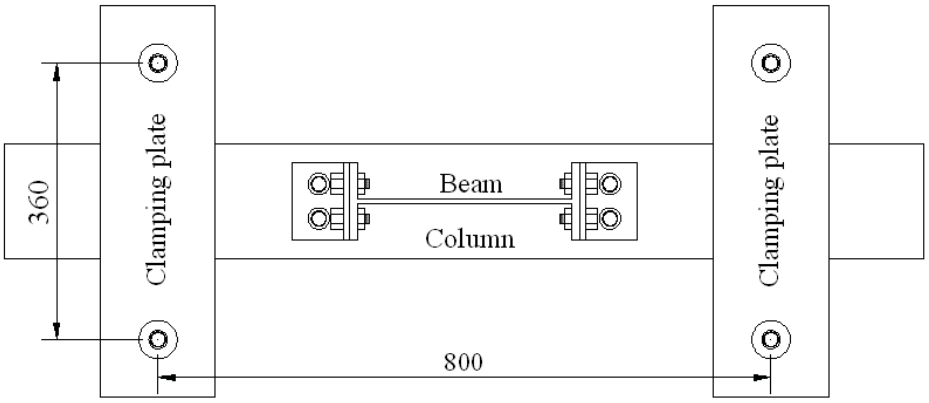

(b) Plane View

Figure 2: Compression test set-up (dimensions in mm)

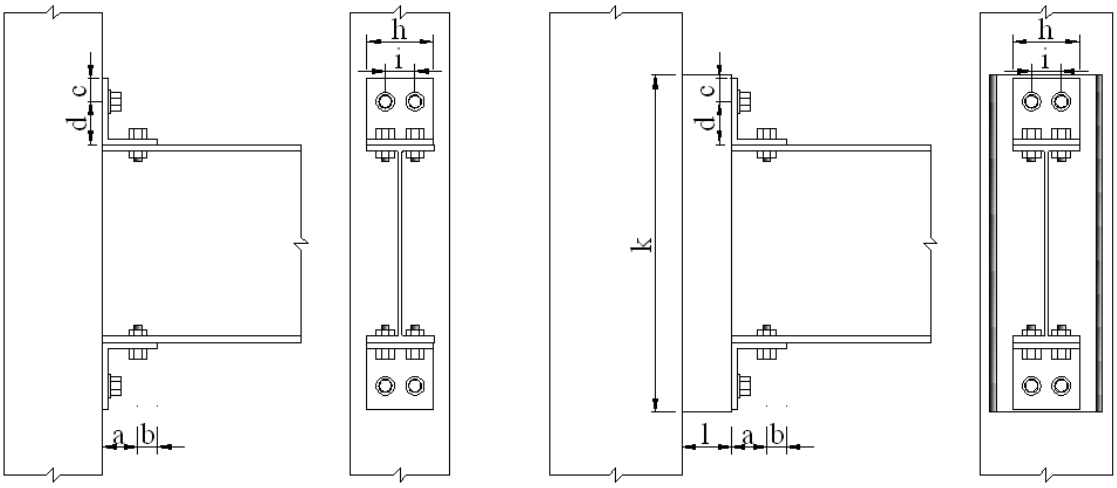

(a) Type A (b) Type B

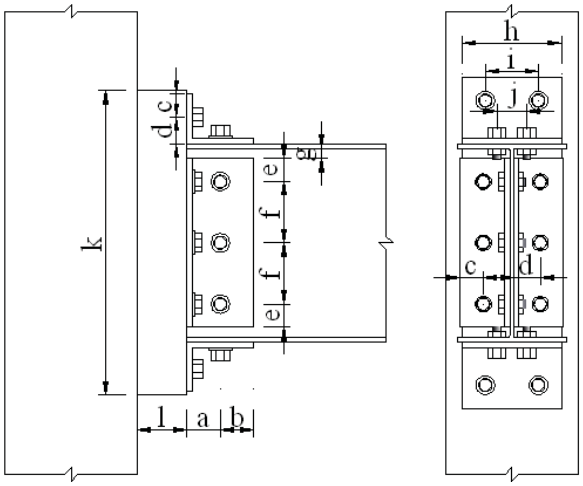

(c) Type C

Figure 3: Configuration of connection specimens

(a) Specimen T1

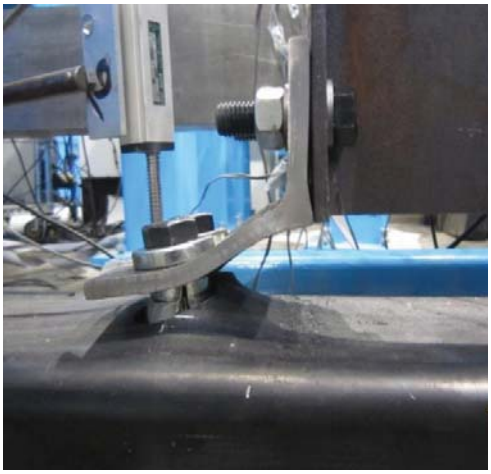

(b) Specimen T2

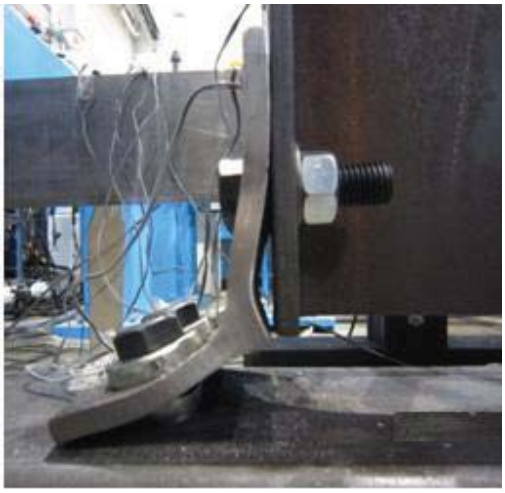

(c) Specimen T3

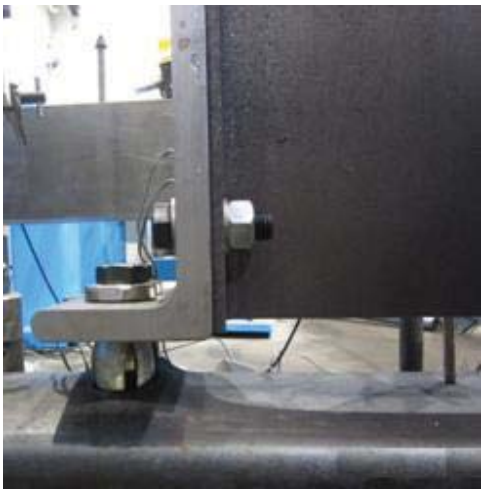

(d) Specimen T4

Figure 4: Main deformation patterns of blind-bolted angle connections under tension

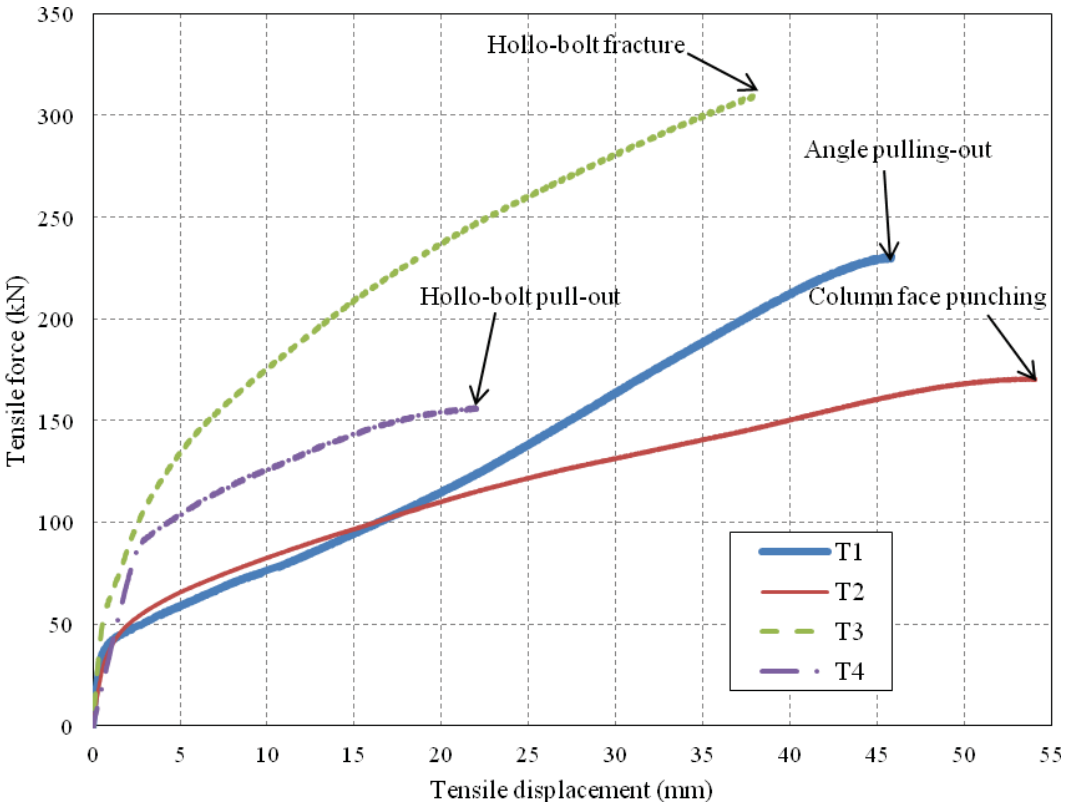

Figure 5: Tensile force-displacement relationships for blind-bolted angle connections

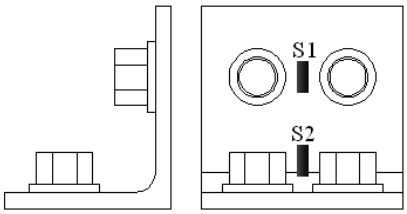

Lateral view Front view

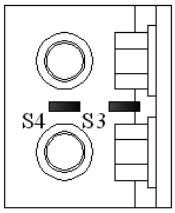

Plan view

(a) Location of stain gauges in the angle

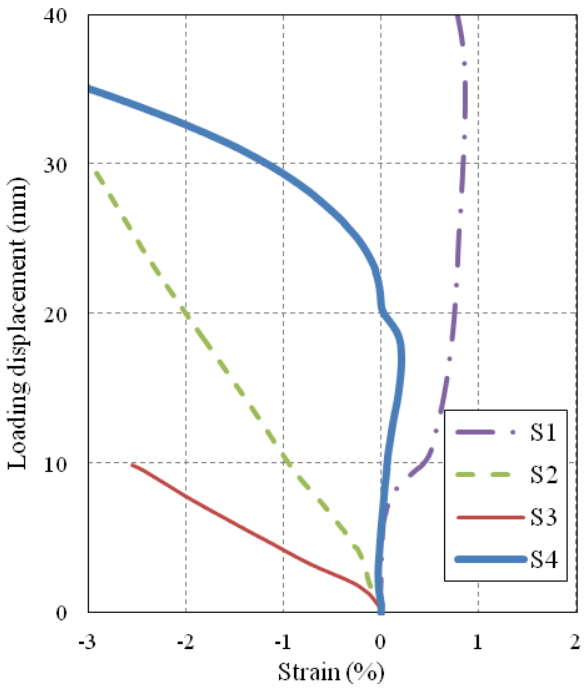

(b) Specimen T1

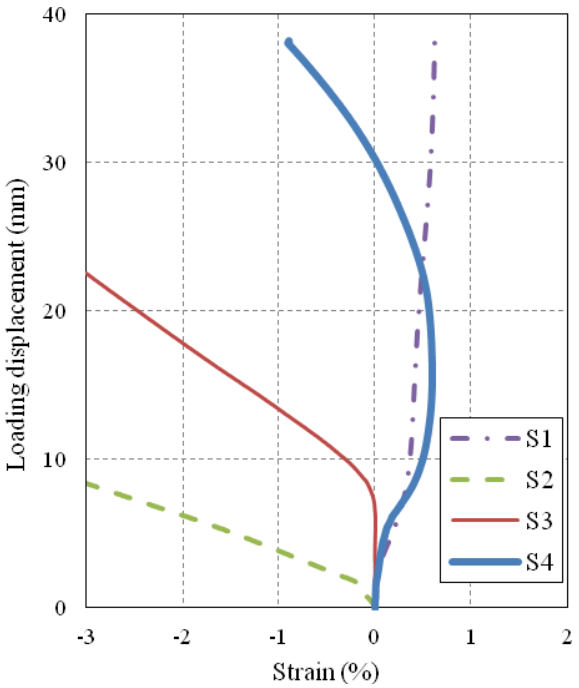

(c) Specimen T3

Figure 6: Strains in angles in Specimens T1 and T3 under tensile force

(a) Specimen T5

(b) Specimen T6

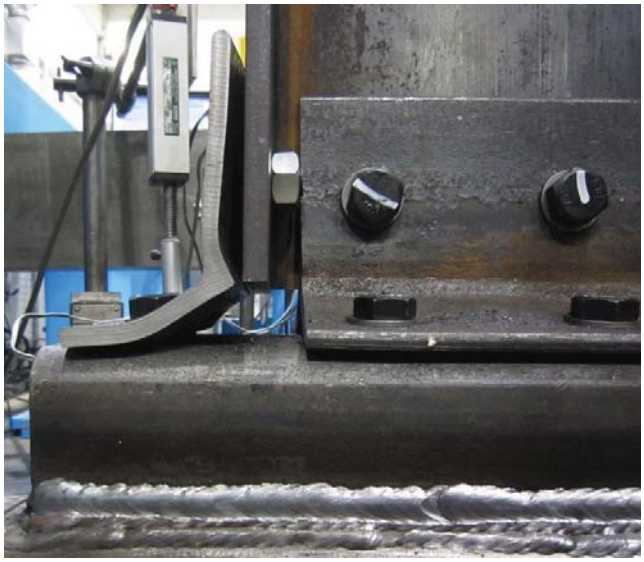

(c) Specimen T7

Figure 7: Main deformation patterns of combined channel/angle connections under tension

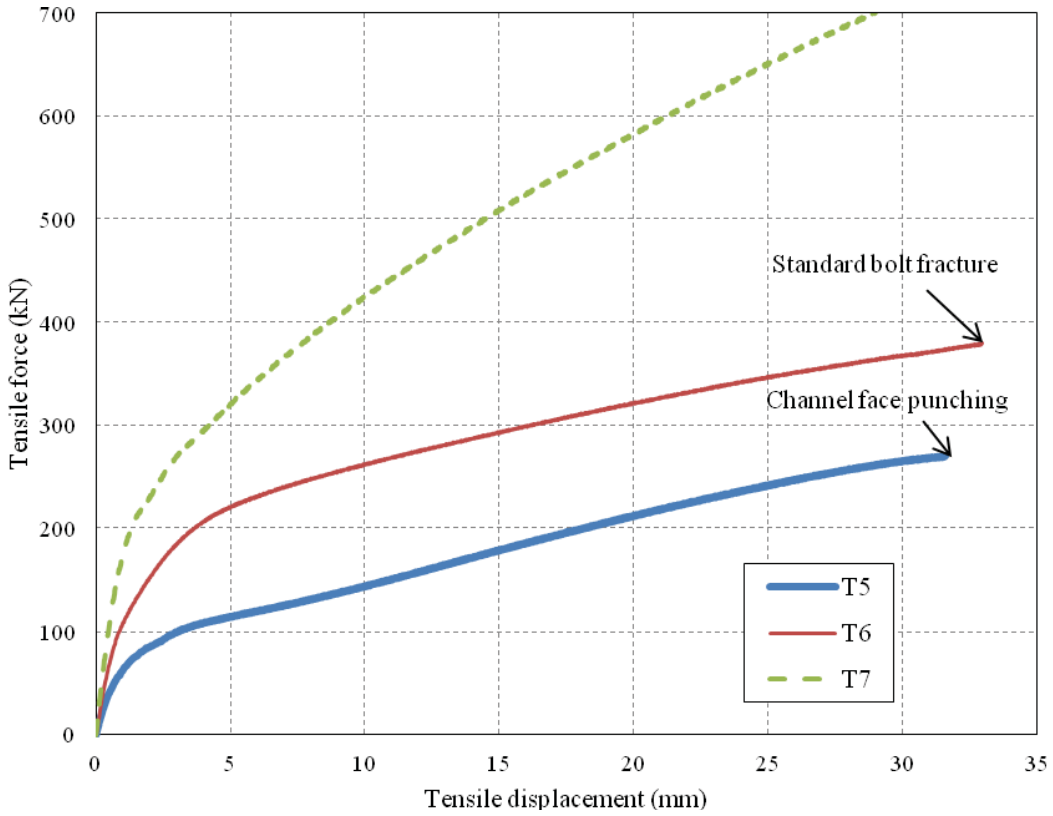

Figure 8: Tensile force-displacement relationships for combined channel/angle connections

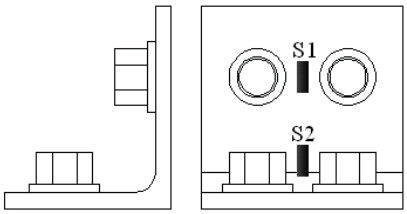

Lateral view Front view

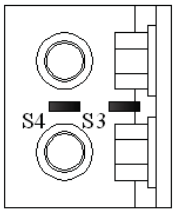

Plan view

(a) Location of stain gauges in the angle

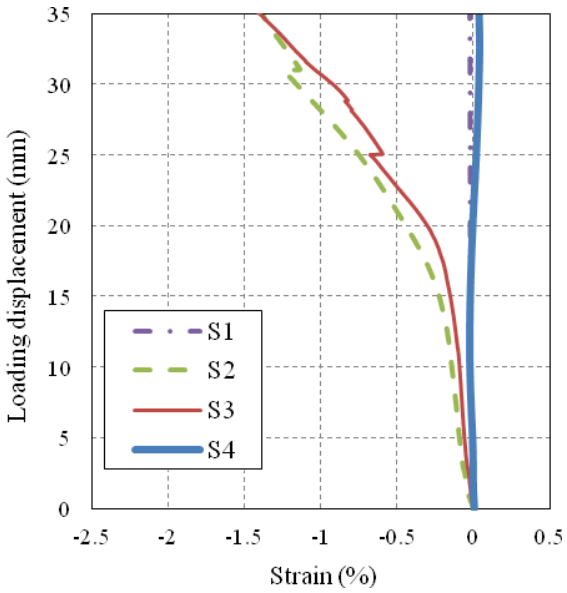

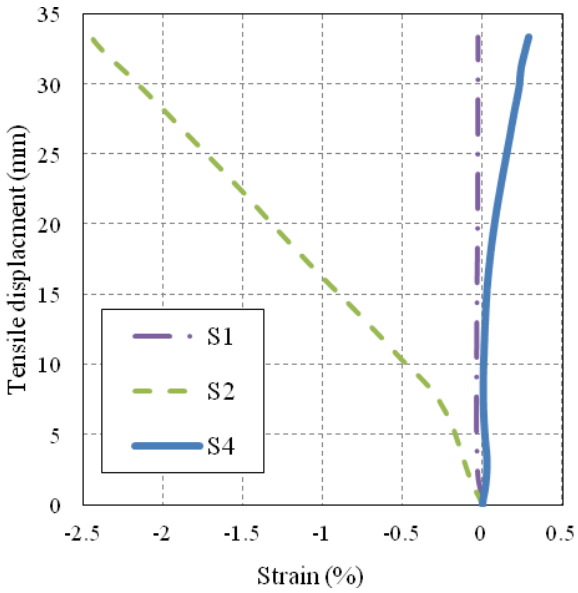

(b) Specimen T5 (c) Specimen T6

Figure 9: Strains in angles in Specimens T4 and T5 under tensile force

Angle Column

(a) Specimen C1

Angle Column

(b) Specimen C2

Angle Column

(c) Specimen C3

Figure 10: Main deformation patterns of angle and column in blind-bolted angle connections at the end of compression tests

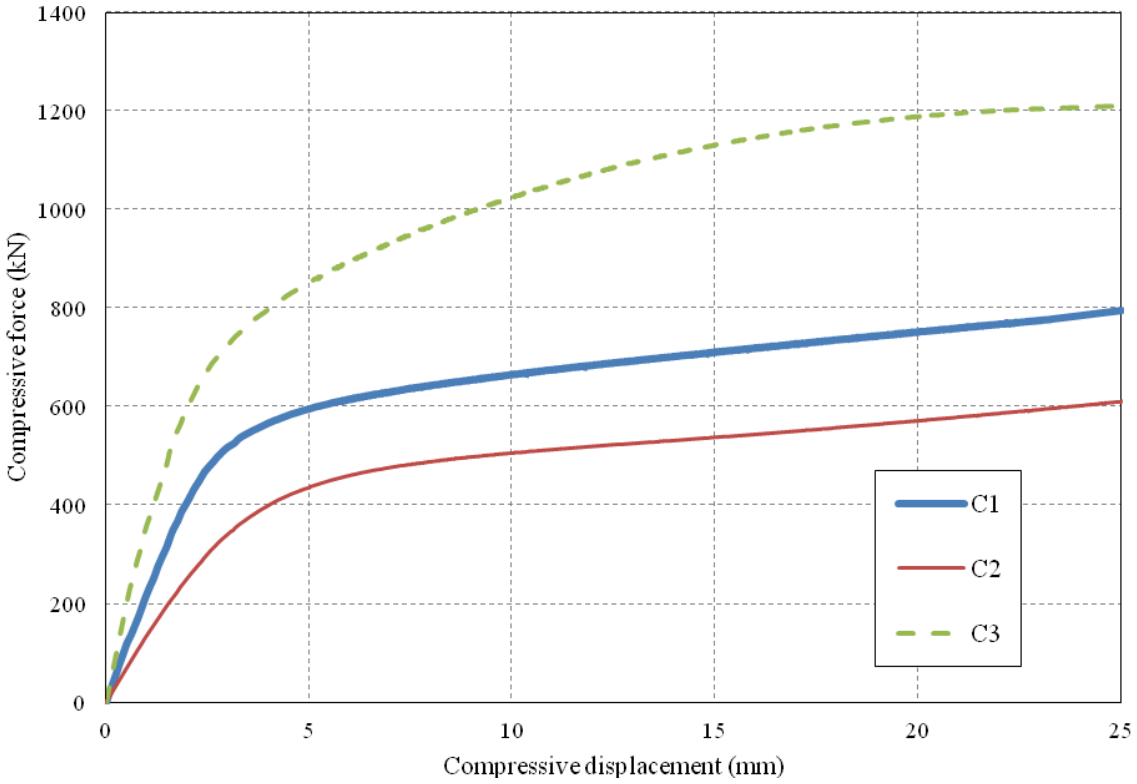

Figure 11: Compressive force-displacement relationships for blind-bolted angle connections

Angle

Channel

(a) Specimen C4

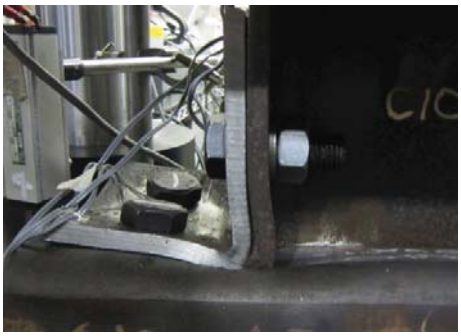

Angle

Channel

(b) Specimen C5

Angle

Channel

(c) Specimen C6

Figure 12: Main deformation patterns of angle and column in combined channel/angle connections at the end of compression tests

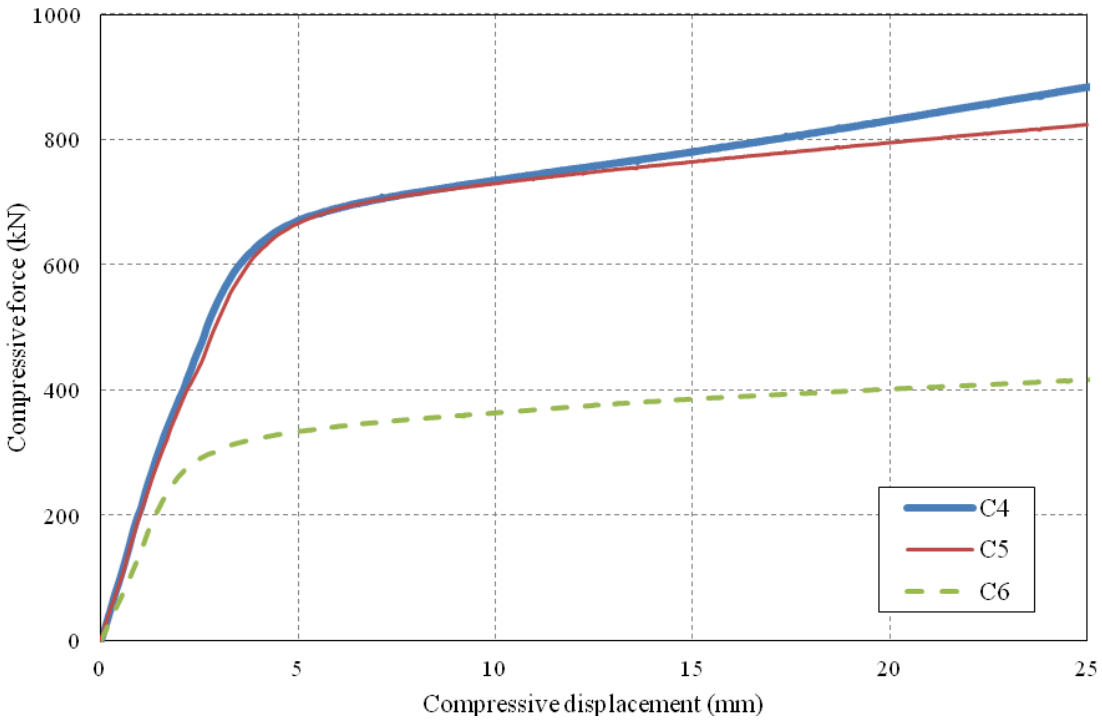

Figure 13: Compressive force-displacement relationships for combined channel/angle connections

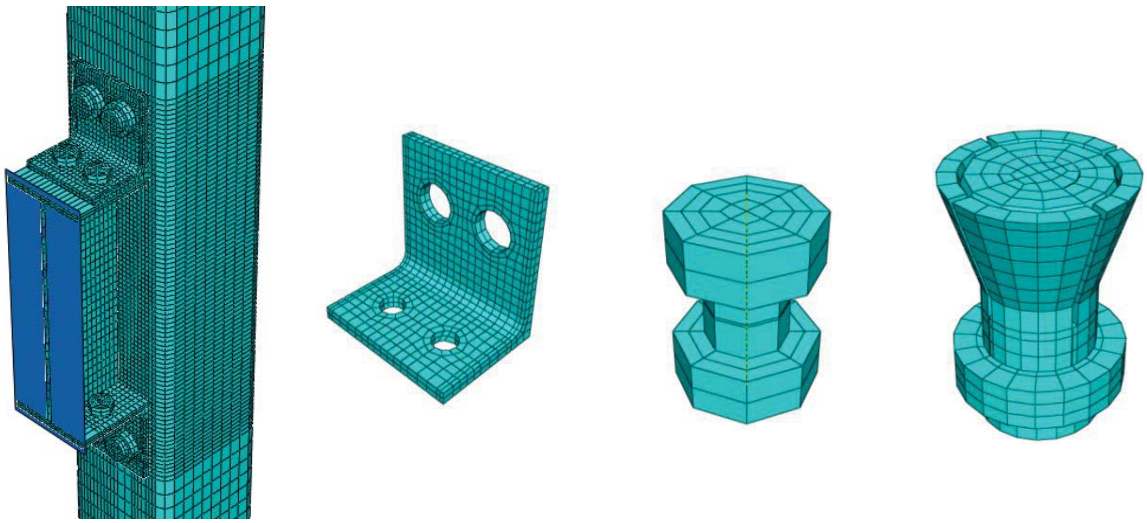

(a) Overall Connection (b) angle (c) standard bolt (d) Hollo-bolt

Figure 14: Views of the finite element model

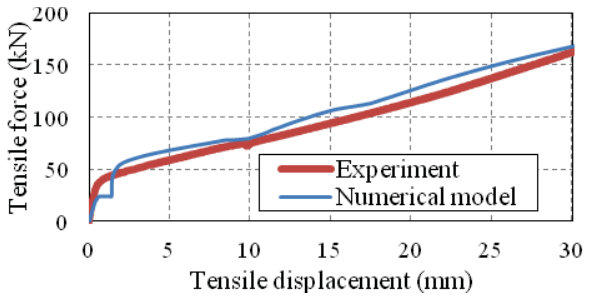

(a) Specimen T1

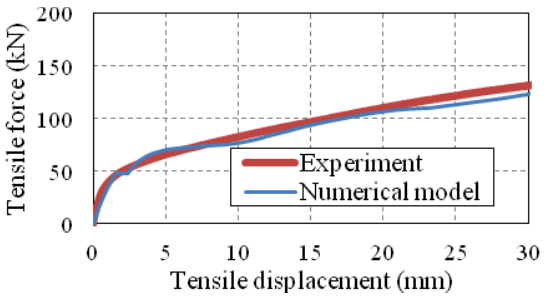

(b) Specimen T2

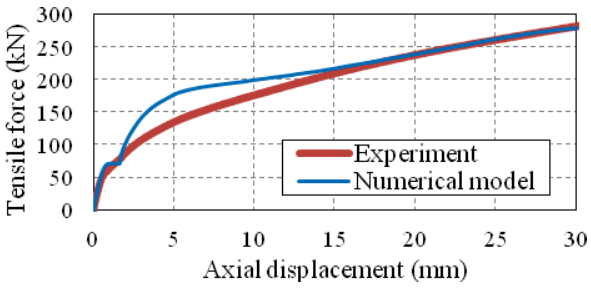

(c) Specimen T3

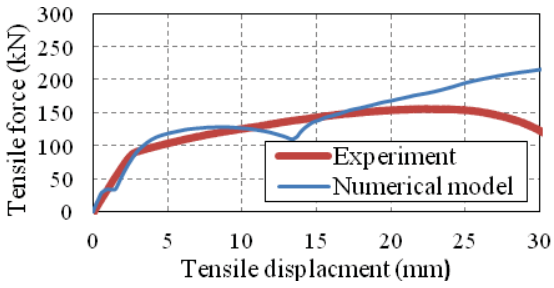

(d) Specimen T4

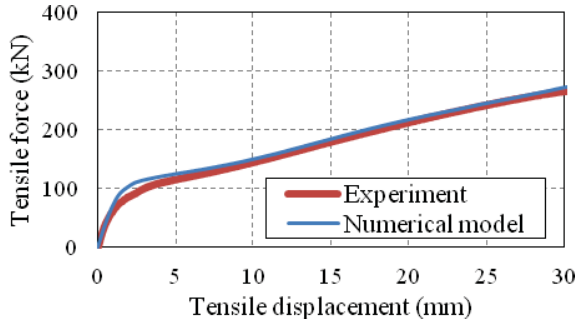

(e) Specimen T5

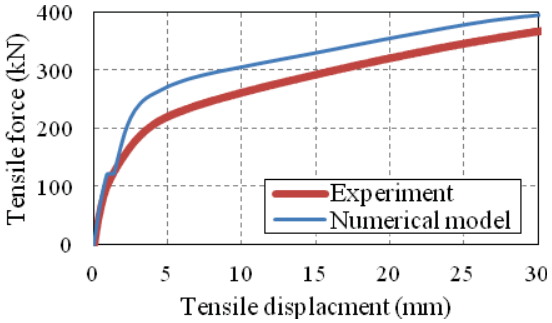

(f) Specimen T6

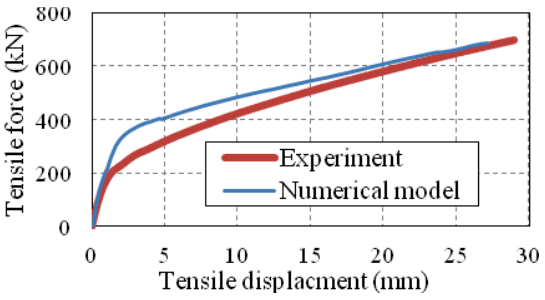

(g) Specimen T7

Figure 15: Comparison of experimental and predicted tensile force-displacement relationships for bolted angle connections

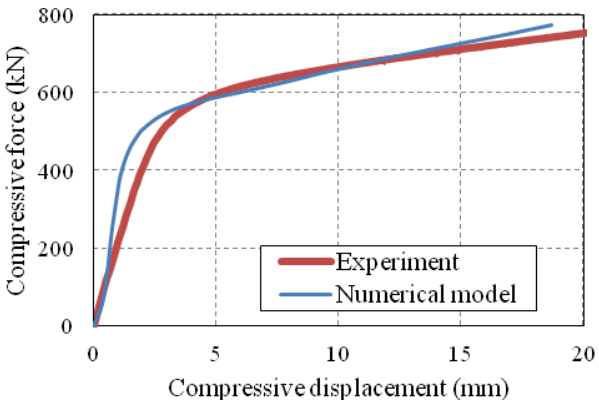

(a) Specimen C1

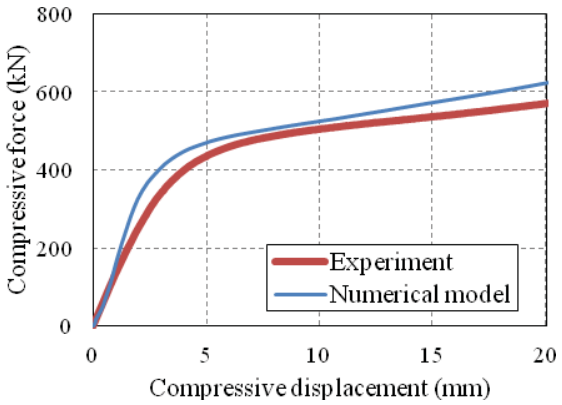

(b) Specimen C2

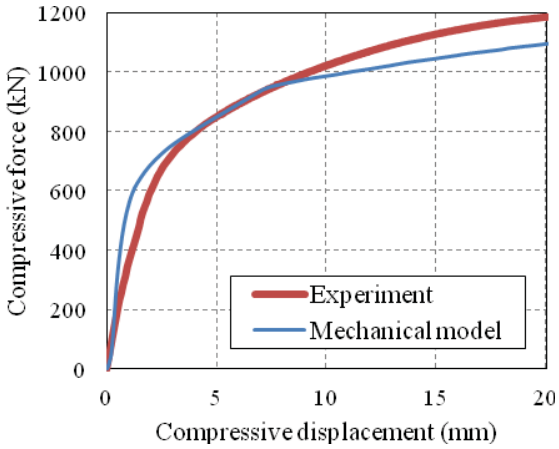

(c) Specimen C3

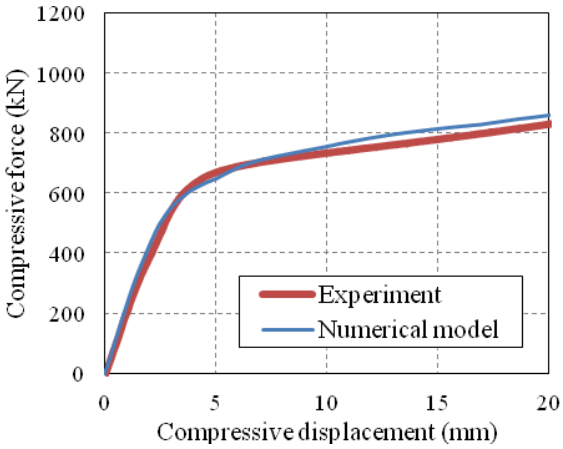

(d) Specimen C4

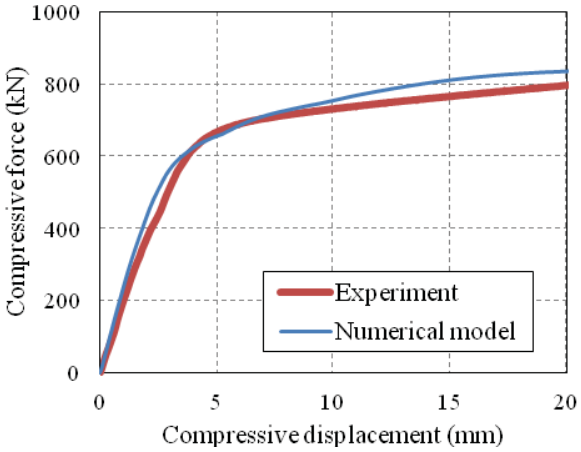

(e) Specimen C5

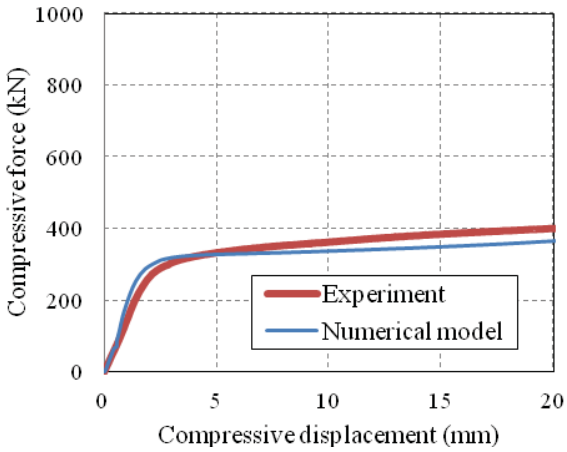

(f) Specimen C6

Figure 16: Comparison of experimental and predicted compressive force-displacement relationships for bolted angle connections

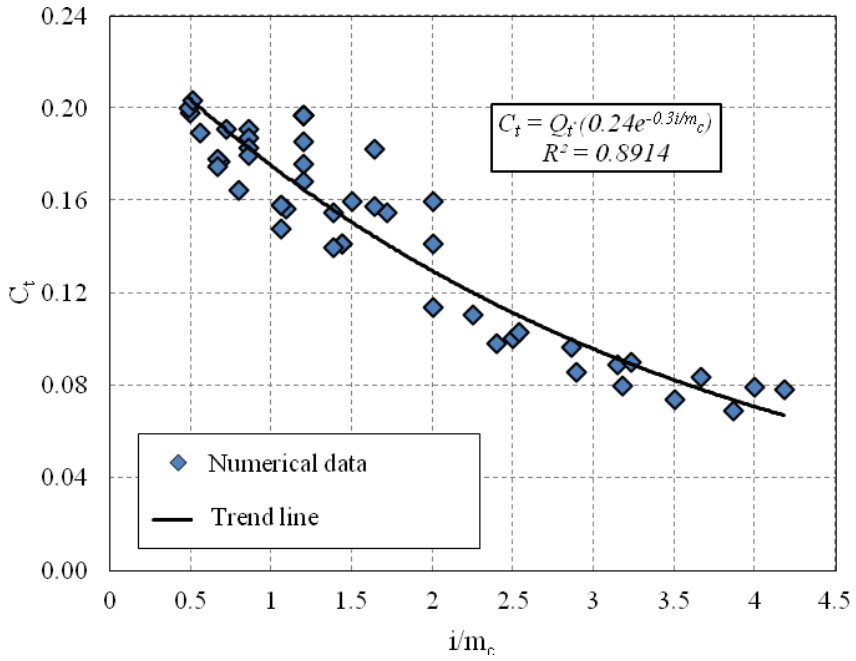

(a) Relationship between C_t and i/m_c (for $L>100mm$)

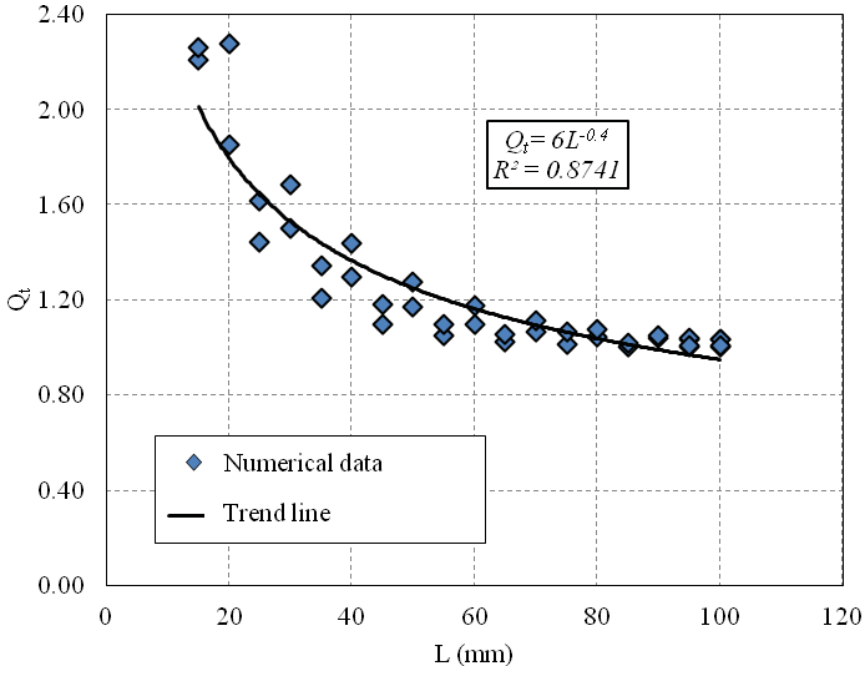

(b) Relationship between Q_t and L (for $L\leq100mm$)

Figure 17: Variation of C_t as a function of geometry

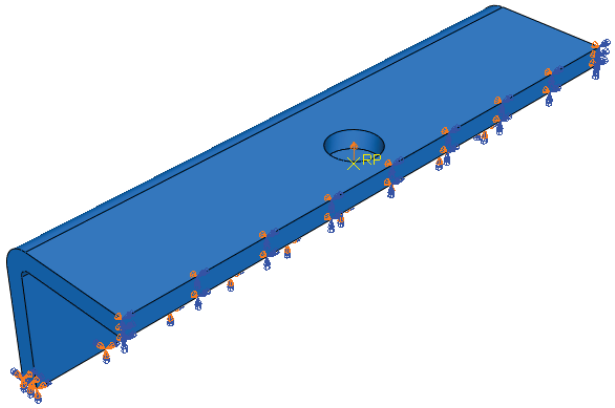

(a) FE model

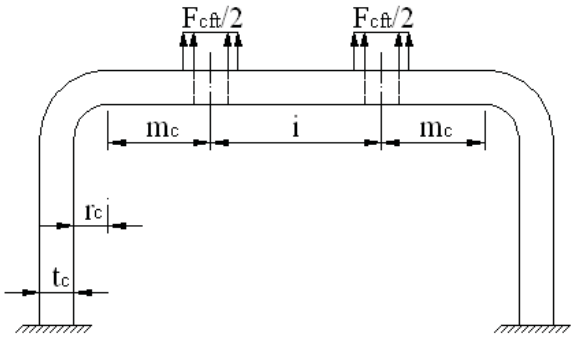

Front view

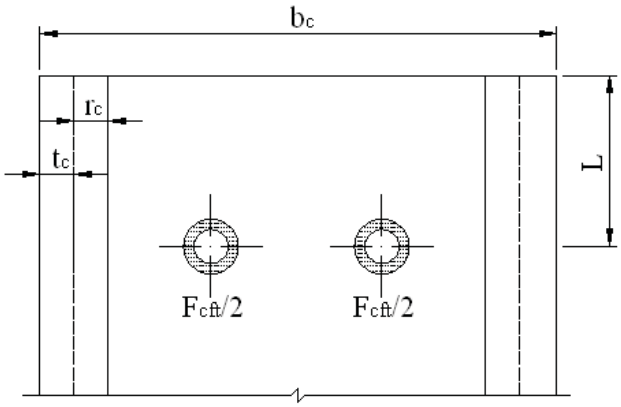

Plane view

(b) Schematic representation

Figure 18: FE models for column face in tension

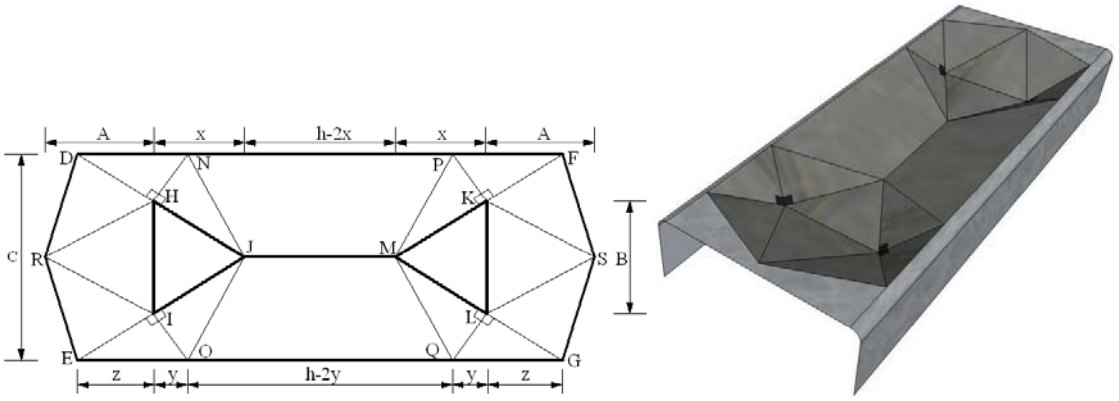

Plan View 3D View

(a) Column/channel yield mechanism

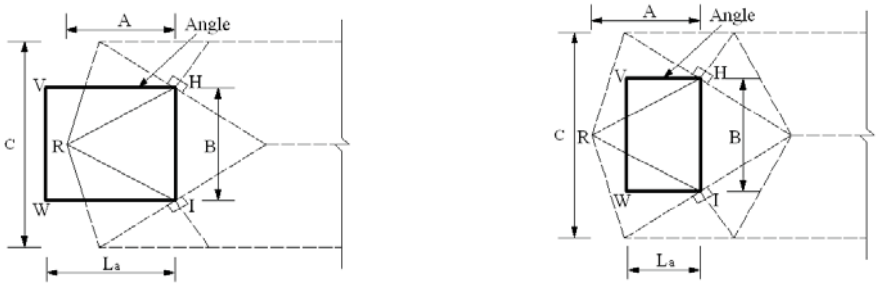

Case A Case B

(b) Angle yield mechanism

Figure 19: Yielding Mechanism 1 of column/channel face and angle in compression

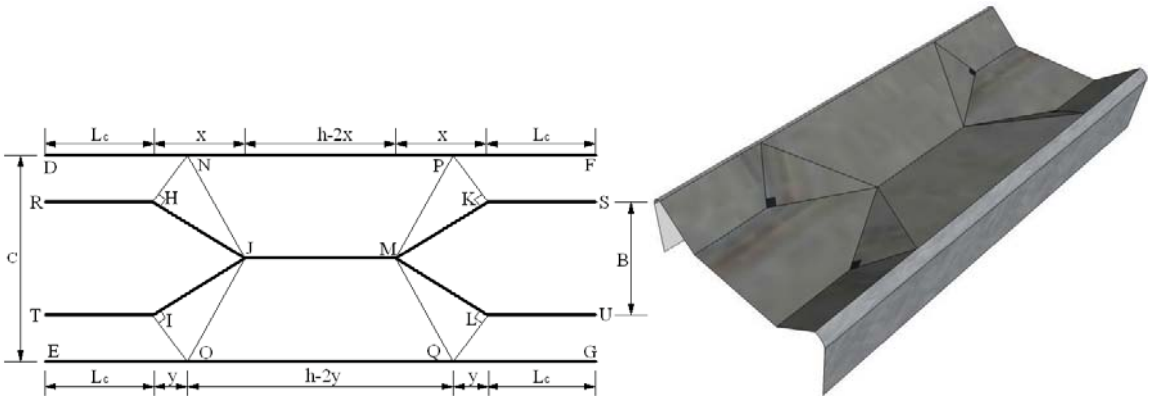

Plan View 3D View

Figure 20: Yielding Mechanism 2 of channel face in compression

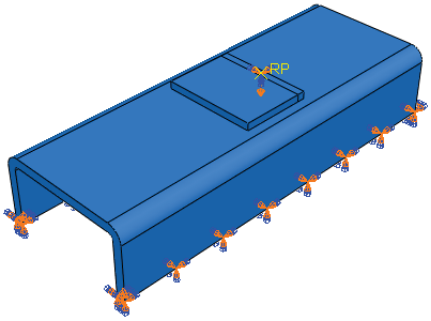

(a) FE model

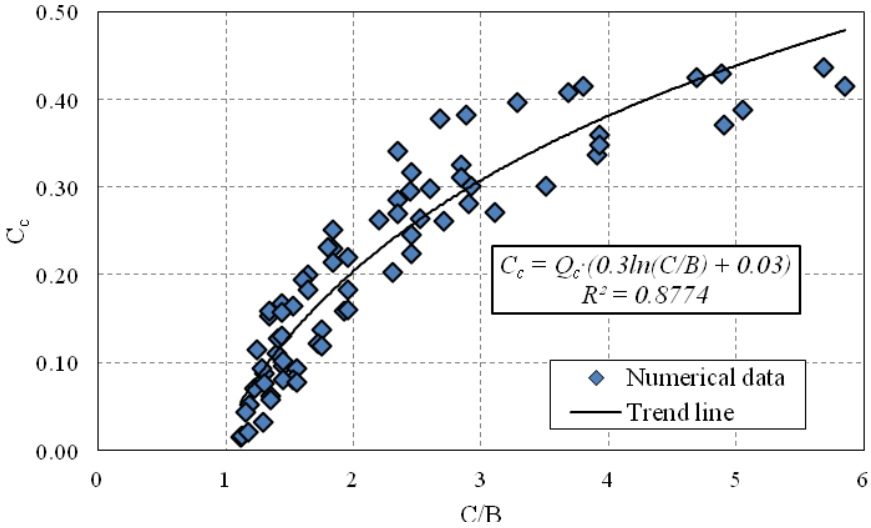

(b) Relationship between C_c and C/B (for L_c >100 mm)

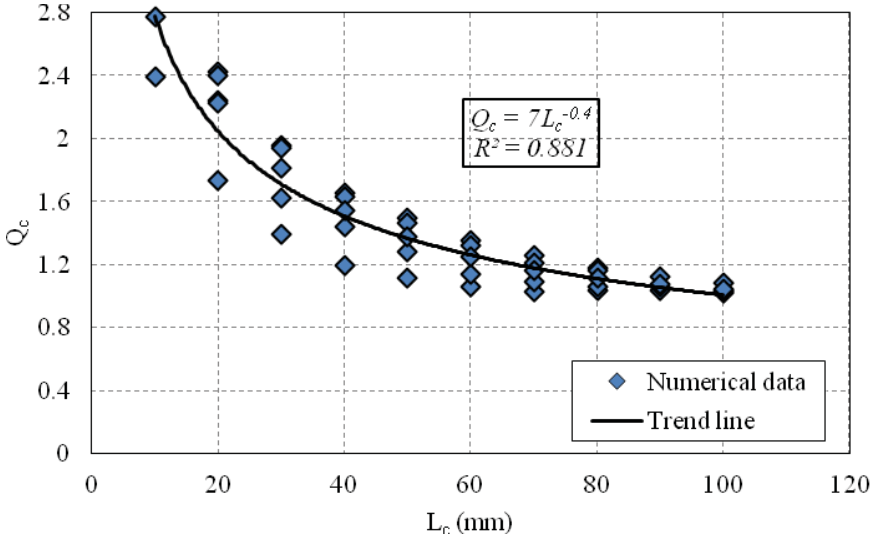

(c) Relationship between Q_c and L_c (for $L_c \leq 100$ mm)

Figure 21: Determination of the stiffness coefficient C_c for column/channel face in compression

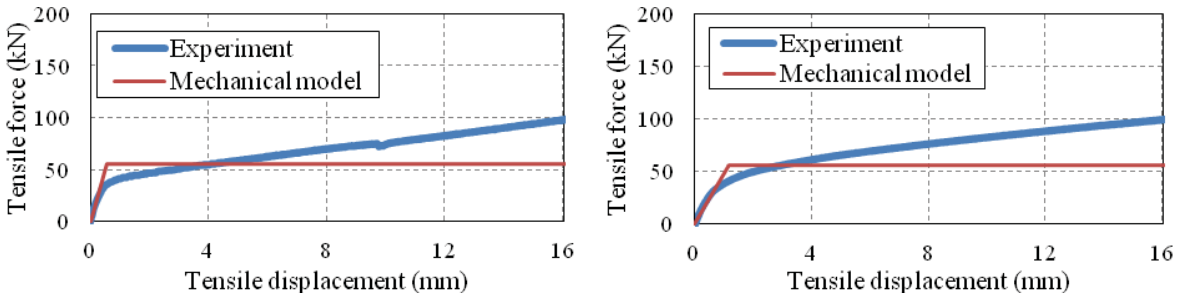

(a) Specimen T1

(b) Specimen T2

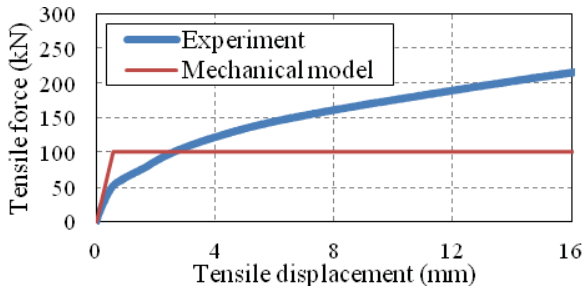

(c) Specimen T3

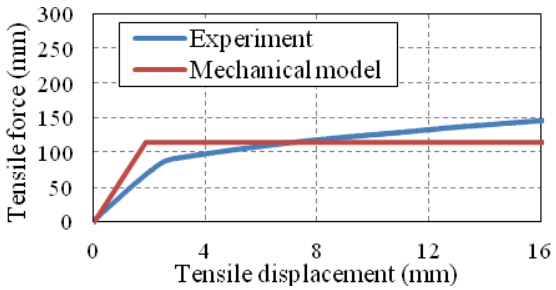

(d) Specimen T4

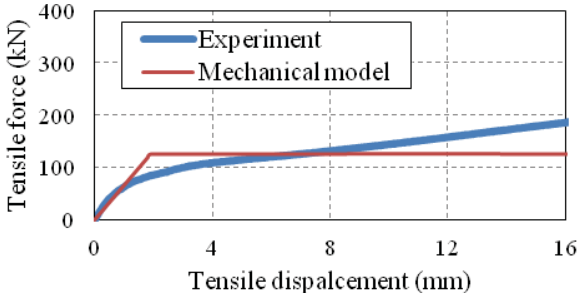

(e) Specimen T5

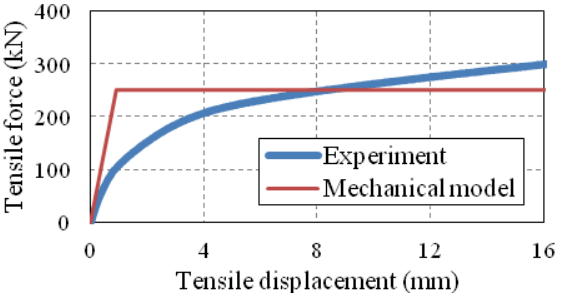

(f) Specimen T6

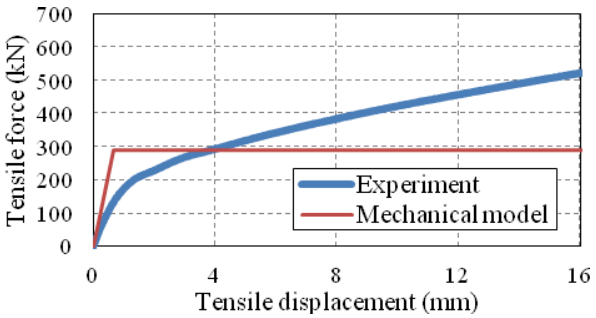

(g) Specimen T7

Figure 22: Comparison of tensile force-displacement relationships for bolted angle connections between test and mechanical model

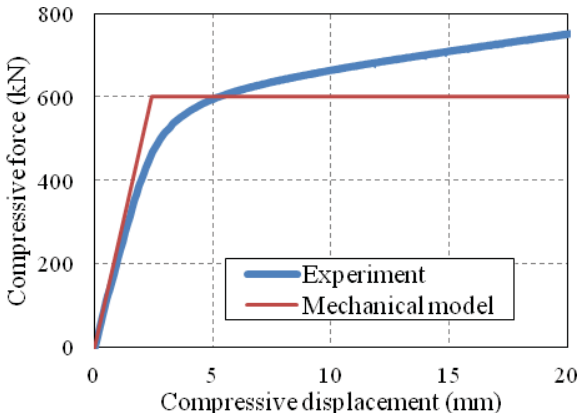

(a) Specimen C1

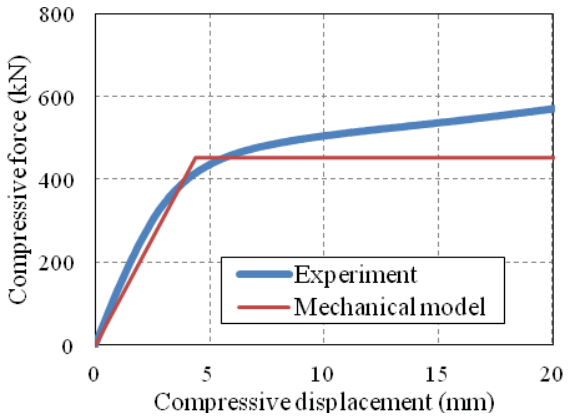

(b) Specimen C2

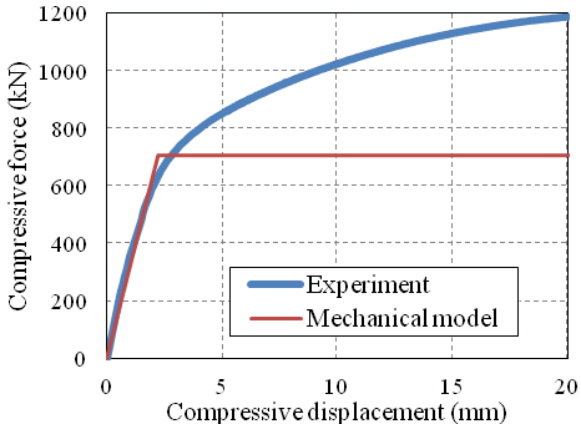

(c) Specimen C3

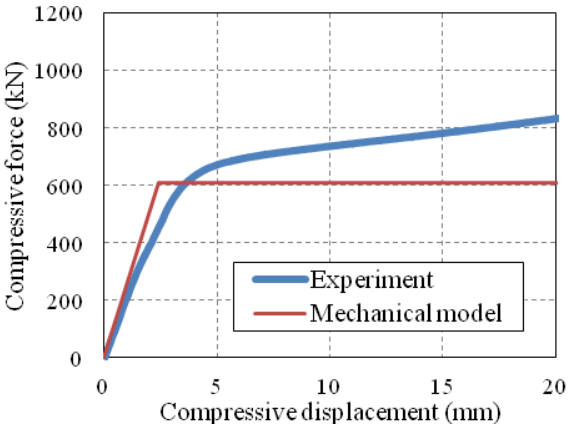

(d) Specimen C4

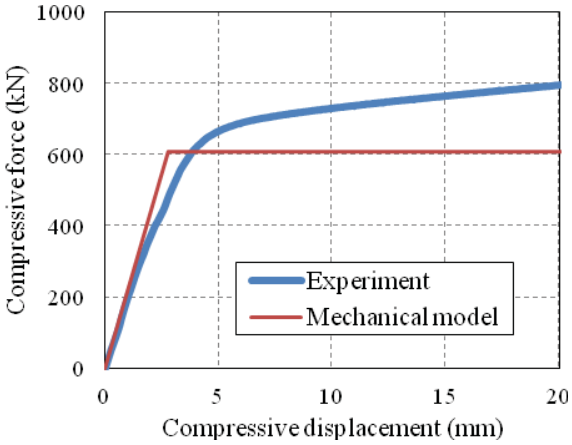

(e) Specimen C5

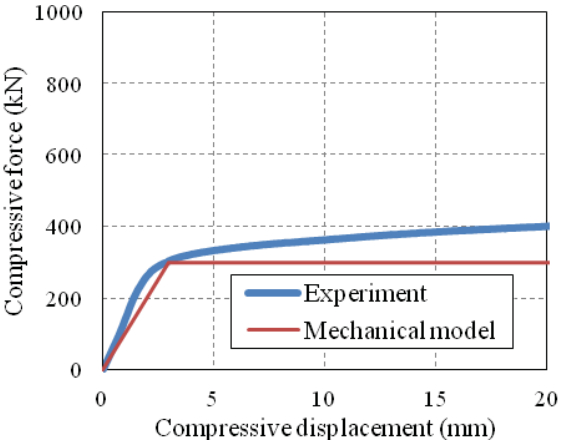

(f) Specimen C6

Figure 23: Comparison of compressive force-displacement relationships for bolted angle connections between test and mechanical model